Plant-soil-water interactions: Implications from U-Th-Ra isotope analysis in soils, soil solutions and vegetation (Strengbach CZO, France)

François Chabaux, Peter Stille, Jonathan Prunier, Sophie Gangloff, Damien Lemarchand, Gilles Morvan, Justine Négrel, Eric Pelt, Marie-Claire Pierret, Sophie Rihs, et al.

Plant-Soil-water interactions: implications from U-Th-Ra isotope analysis in soils, soil solutions and vegetation (Strengbach CZO, France)

Chabaux François[1*], Stille Peter[1*], Prunier Jonathan[1,2*], Gangloff Sophie[1], Lemarchand Damien[1], Morvan Gilles[1], Négrel Justine[1], Pelt Eric[1], Pierret Marie-Claire[1,] Rihs Sophie[1], Schmitt Anne-Désirée[1], Trémolières Michèle[1,3], Viville Daniel[1].

1- Laboratoire d'Hydrologie et de Géochimie de Strasbourg (LHyGeS), Université de Strasbourg, CNRS, ENGEES, 1 rue Blessig, 67000 Strasbourg, France.

2- Present address: Laboratoire des Sciences du Bois, UMR EcoFoG, CNRS, Campus Agronomique de Kourou, BP 316, 97387 Kourou, France.

3- Present address: Laboratoire Image, Ville, Environnement (LIVE), Université de Strasbourg, CNRS, ENGEES, 3 rue de l'Argonne, 67000, Strasbourg, France.

*Corresponding authors:
fchabaux@unistra.fr , pastille@unistra.fr, Jonathan.Prunier@ecofog.gf

Keywords: ^{238}U-^{234}U-^{230}Th-^{226}Ra radioactive disequilibria, $^{230}Th/^{232}Th$ activity ratios, soils, soil solutions, vegetation, Strengbach catchment.

ABSTRACT

This study presents U-Th-Ra isotope data for soils, soil grain size fractions, soil solutions, throughfall, rainwater and tree samples from two experimental plots under spruce and beech trees, in the Strengbach catchment (France) that highlight the importance of the ^{238}U-^{234}U-^{230}Th-^{226}Ra nuclides and the ($^{230}Th/^{232}Th$) for the tracing of biogeochemical cycles in the plant-soil-water system of the critical zone (CZ).

The results highlight the very contrasting impact of trees on the U-Th and Ra (Ba) budgets in forest ecosystems with Ra-Ba being strongly and U-Th very little cycled by vegetation, leading to high ($^{226}Ra/^{230}Th$) and ($^{226}Ra/^{238}U$) in trees. Thorium-Ra(Ba) fractionations in soil solutions and soils are therefore strongly influenced by tree uptake and litter decay but U-Th fractionations are little influenced. Compared to other classical isotope systems such as Sr or Nd that are routinely used in the study of the CZ and significantly affected by vegetation cycling, U-Th isotopes are probably among the few tracers to be specific tracers of water-rock interactions in the CZ. The Th activity ratios of soil minerals, especially of minor and secondary mineral phases, show a large range of variation, from 0.7 to 5 in the Strengabch case. These different characteristics give Th activity ratio an important role for tracing the sources of chemical fluxes in soils, soil solutions and vegetation that is currently under-exploited. The Strengbach study illustrates the utility of this approach and the methodology is further strengthened by the combination of U, Th activity ratios and Sr isotope ratios, which also provides additional constraints on the weathering processes affecting the Strengbach bedrocks and the nature of the reservoirs involved in the plant-soil-water transfers. The results emphasize that minor mineral phases such as zircon, sulfate and phosphate are important sources of the U-Th fluxes transiting soil solutions and significantly control the U and Th budget of the Strengbach soil samples and their Th activity ratios. Furthermore, the comparison of the U-Th-Sr isotopic characteristics of soil solutions and soil grain size fractions allows the recognition of two stages of weathering of the bedrock i.e. 1- dissolution of the primary minerals and formation of the secondary ones in the deep soil horizons, and 2- dissolution of both primary and secondary minerals mainly from the finest soil grain size fractions in the nearest surface soil horizons. The latter might be related to recent modifications of the weathering processes in the

catchment, stronger and older under the spruce than the beech plot. We propose that degree of weathering modification is related to the nature of tree cover because spruce plantations have caused an increase of soil acidity and hence of weathering intensity of some minerals and likely also of Ca leaching from the Ca-poor Strengbach soils over the past decades. The U-Th-Sr results of this study also point to the occurrence of isotopically different reservoirs of these elements for trees and gravity soil solutions collected by lysimetric plates. This further suggests that for the Strengbach watershed the gravity soil solutions cannot be the main tree nutrient reservoir.

1. INTRODUCTION

Soil horizons play a key role in the evolution of the critical zone, as dynamic and porous interfaces that connect the atmosphere, vegetation, rocks, groundwaters and surface waters (Banwart et al., 2017; 2019). Precise knowledge of the relationships and inter-relationships between the different components of this highly complex system is necessary when one seeks, for instance, to model precisely the soil and critical zone evolution (Banwart et al., 2019) or the chemical composition of stream and surface waters (e.g., Li et al., 2017; Lucas et al., 2017; Ackerer et al., 2018). Knowledge of key parameters including the nature and extent of weathering processes active in the soil horizons and the interplay between biological processes, water circulation and water-rock interactions, is certainly still insufficient. Advances in the description/understanding of the main key hydro-biogeochemical reservoirs and processes that are active in the surface soil horizons are still required.

Geochemical and especially isotopic approaches have been developed to address these issues, both to specify the sources of elements and constrain their pathways in plant-soil-water systems (e.g., Blum and Erel, 2005; Bouchez et al., 2013; Bullen and Kendall, 1998; Kendal and Doctor, 2005). Significant efforts have been made over recent decades to evaluate the potential of using geochemical proxies for hydrogeochemical processes and biogeochemical cycles active within the soil system. Understanding the parameters and processes that control the behavior of geochemical tracers during plant-soil-water interactions has progressed from studies conducted at the experimental watershed scale down to the laboratory experiment scale. Such studies have included a large number of geochemical tools: trace elements, traditional and non-traditional stable isotopes, and radioactive and radiogenic isotopes (e.g., Akerman et al., 2014; Aubert et al., 2001; 2002; Babcsányi et al., 2014; 2016; Braun et al., 1998; Bouchez et al., 2013; Bullen and Eisenhauer, 2009; Chabaux et al. 2015a,b; Cividini et al., 2010; Ladouche et al., 2001; Laveuf and Cornu, 2009; Ma et al., 2011; Négrel et al., 2018; Opfergelt and Delmelle, 2012; Opfergelt et al., 2014; Schmitt et al., 2003, 2012; 2013; Steinmann and Stille, 1997; 2009; Stille et al., 2006; 2009; 2011; Viers et al., 2015; Voinot et al., 2013).

These different studies have emphasized the potential of using these geochemical tools to characterize biogeochemical cycles and hydrogeochemical transfer in plant-soil-water systems. These studies also clearly demonstrated interest in coupling

geochemical proxies in water, soils and vegetation to understand the critical zone processes and their dependence on environmental conditions (e.g., Sullivan et al. 2016 and references therein).

In the framework of these efforts, little attention has been paid so far to ^{238}U-^{234}U-^{230}Th-^{226}Ra nuclides and to Th isotope ratios as potential proxies/tracers of critical zone function. To date, studies on U-series nuclides in soils, surface waters and sediments have been mainly undertaken to determine the time constants of alteration and erosion processes in the critical zone (e.g., Ackerer et al., 2016; Bourdon et al., 2009; DePaolo et al., 2006; 2012; Dequincey et al., 2002; Chabaux et al., 2003a,b; 2012; 2013; Gontier et al., 2015; Maher et al., 2006; Pelt et al., 2008; Dosseto et al., 2008; 2014; Dosseto and Schaller, 2016; Ma et al., 2010; 2012; 2013; Vigier et al., 2001). However, few studies have suggested the potential of using ^{238}U-series nuclides to trace hydro- and biogeochemical transfers in watershed and soils. For instance, the coupling between U and Sr isotopes has successfully elucidated the hydrogeochemical fluxes in watershed and soil solutions (Riotte and Chabaux, 1999; Bagard et al., 2011; Chabaux et al., 2001; Riotte et al., 2003; Durand et al., 2005; Pierret et al. 2014; Schaffhauser et al., 2014; Prunier et al., 2015; Tricca et al., 2001). The ($^{230}Th/^{232}Th$) activity ratios (hereafter, activity ratios will be noted in brackets) in the different rock minerals were also observed to span a large range of values (Bosia et al., 2016; 2018) that could thus, once combined with Sr or Nd isotopes, be relevant to characterize the mineralogical source of elements in watersheds. Finally, several studies have indicated the potential impact of vegetation on the Ra geochemical cycle (e.g., Cerne et al., 2010; Gerzabeck et al., 1998; Greeman et al., 1999; Jeambrun et al., 2012; Million et al., 1994; Pourcelot et al., 2017; Rihs et al., 2011; 2016; Soudek et al., 2004; Lascar, 2019). These results suggest that ^{238}U-^{234}U-^{230}Th-^{226}Ra nuclides and ($^{230}Th/^{232}Th$) ratios are anticipated to be relevant for tracing sources of elements, weathering processes and hydrogeochemical pathways in the plant-soil-water system. So, in this study these nuclides along with the ($^{230}Th/^{232}Th$) were analysed in the soils, soil solutions and trees of the Strengbach Critical Zone Observatory (http://ohge.unistra.fr) in order to constrain better their contribution to our understanding of the plant-soil-water system. The Strengch CZO is an instrumented watershed, very well suited for this type of work, as already illustrated for other geochemical tools, because it allows for the different

hydrogeological and biological components involved in plant-soil-water transfers to be sampled (e.g., Aubert et al., 2004; Gangloff et al., 2014; Lemarchand et al., 2010; Stille et al., 2006; 2009; 2011; 2012; Tricca et al., 1999; Cenki-Tok et al., 2009; Cividini et al., 2010; Lemarchand et al., 2010; Lemarchand et al., 2012; Schmitt et al., 2003; 2017; 2018).

2. SITE AND SAMPLING

2.1. Site description

The uppermost Strengbach watershed (0.8 km^2) is situated in the Vosges mountains (northeastern France) at altitudes between 880 and 1150 m (a.m.s.l.) and has relatively steep slopes (mean 15°) (Fig. 1). This area is an instrumented environmental observatory (http://ohge.unistra.fr) involved in the French critical zone observatories network OZCAR (French network of Critical Zone Observatories: Research and Applications) (http://www.ozcar-ri.org), where meteorological, hydrological and water chemistry data have been collected since 1986 (e.g., Viville et al., 2012; Pierret et al., 2014; 2018 for additional details). It was recently used to carry out a study of in-situ dissolution rates of silicate minerals in the critical zone (Wild et al., 2019). The climate is temperate oceanic mountainous with an average rainfall of 1400 $mm.yr^{-1}$, with ≈20% under snowfall. Forest covers 90% of the geographical area of the watershed. The forest area is composed of 80% spruces (*Picea abies L.*) and 20% beeches (*Fagus sylvatica*).

The bedrock is mainly composed of Hercynian base-poor granites (the Brezouard granite Massif), locally marked by petrological and mineralogical variabilities linked to the polyphased history of these granites. As detailed in Hasalova et al. (2015) and Tabaud et al. (2015), granites are derived from two main generations of granitic magmas: a first and extensive K-Mg granitoid magmatism around 340 Ma, followed by magmatic events occurring at ca. 325 Ma, which produced a large amount of felsic anatectic melts, which pervasively intruded and compositionally and texturally reworked previously formed granitoids (in Hasalova et al., 2015). Such a magmatic history in the Strengbach watershed results in a continuum between porphyritic granites with large feldspars and plagioclase phenocrysts, which were formed during the first magmatic stage, to fine-grained more isotropic granites,

which were formed by crystallization of the late felsitic magmas, via intermediate granites where the two magmatic assemblages are recognizable. Such a magmatic history can lead to the coexistence of different types of K-feldspars in the same rock, with Ba-rich K-feldspars crystallized from the primary magmas and Ba-poor K-feldspars recrystallized from secondary anatectic magmas (Hasalova et al., 2015). The granitic bedrock has undergone late hydrothermal alterations, which are more important on the northern slope of the catchment than on the southern slope (Fichter et al., 1998 a,b). Field observations also indicate the occurrence of more or less developed veinlets of secondary minerals, including Fe and Mn oxyhydroxides, quartz, and barite, which can be related to hydrothermal or meteoritic alterations. Some of the meteoritic alterations might be of ante-Triassic age (Wyns et al., 2004; Dewandel et al., 2006).

A sandy saprolite, which can reach several meters of thickness, usually separates soil and granite. The soils are 80-100 cm deep and vary from Dystric Cambisol to Albic Podzol (brown acidic to ochreous brown podzolic) (WRB 2014). The soils are very coarse-grained, sandy and rich in gravel (Fichter et al., 1998a,b). The shallow soils (upper 50 cm) under spruce (VP site) and beech (HP site) are acidic (pH=3.7-4.5) (Aubert et al., 2001; Solovitch-Vella et al., 2007). Distric Cambisols are mainly located on the northern slope, and Albic Podzols are located on the southern slope. This soil difference likely results from the differences in the lithology, vegetation cover and local climate between the north- and south-facing slopes (e.g., Pierret et al., 2014).

2.2. Sampling

Samples were collected between 2004 and 2006 from two experimental sites: one under spruce trees that were planted between 1890 and 1900, which is locally named the VP site and hereafter the “spruce site”, and the other under beeches that were planted between 1860 and 1870, hereafter named HP or the “beech site” (Location Fig. 1). The beech site is developed on the gently hydrothermally altered granite, while the spruce site has a bedrock that has undergone a much more intense hydrothermal alteration (e.g., Fichter et al., 1998). Fine earth (<2 mm) from two soil layers (30-40 cm and 90-100 cm), which were marked by the highest and weakest root density in the two soil profiles, was collected and separated into four

particle size fractions: < 2 µm (clay), 2-50 µm (silt), 50-100 µm (fine sand) and 1600-2000 µm (coarse sand). Soil solutions were collected by zero-tension lysimeter plates at -5, -10, -30 and -60 cm (noted VP-5, VP-10, VP-30 and VP-60) next to the VP spruce soil profile and at -10 and -70 cm (noted HP-10 and HP-70) next to the HP beech soil profile (see caption Fig. 1). Different parts of spruce and beech trees (sapwood, roots, branches and needles or leaves) and litters from the VP spruce and HP beech sites were collected from 2004 to 2007. Throughfall and rainwater samples were also collected.

3. ANALYTICAL METHODS

3.1. Grain size fractions and granite rocks

Before crushing the fine earth fractions of the four sampled soil horizons, a representative subsample (100 g) was dispersed for 30 min in a cylindrical Pyrex container with 750 ml of ultrapure water to disaggregate the soil and separate the different grain size fractions. The dispersion was sieved at 50 µm through a nylon sieve. The nonpassing fraction was dried at 60°C and used to separate the fine sand (50-100 µm) and coarse sand (1600-2000 µm) fractions using a set of nylon sieves. The clay fraction (<2 µm) and the silt fraction (2-50 µm) was separated from the 50µ-passing fraction via sedimentation in deionized ultrapure water based on Stokes law, followed by centrifugation at 3500 rpm, as detailed in Prunier et al. (2015).

Bedrocks and coarse sands (> 100 µm) of the two soil samples were crushed in an agate disk mill. The major and trace element concentrations of these different samples were measured by ICP-AES (Jobin Yvon) and ICP-MS (VG Plasma Quad Thermo Electron), respectively, after lithium tetraborate fusion. The analytical uncertainty was <3% for major element concentrations and <10% for trace element concentrations at 2σ (Dequincey et al., 2005; Chabaux et al., 2012). For isotopic measurements, an aliquot of approximately 100 mg of granite and particle size fraction powders were spiked with ^{233}U and ^{229}Th tracers and digested by ultrapure HF, HNO_3, $HClO_4$, HCl and H_3BO_3 acids (Pelt et al., 2013). After separation and purification using Biorad AG1x8 anionic resin (e.g., Pelt et al., 2008; Granet et al., 2010), the U-Th concentrations and ($^{234}U/^{238}U$) and ($^{230}Th/^{232}Th$) ratios were measured by thermal ionization mass spectrometry (TIMS, Thermo-Scientific

Triton) using ^{233}U and ^{229}Th tracers. $^{87}Sr/^{86}Sr$ was determined after separation and purification following chromatographic standard procedures on a VG Sector mass spectrometer using a dynamic multicollection (Lahd Geagea et al., 2007). ^{226}Ra concentration measurements were performed by TIMS (Triton Thermo-Scientific) from another powder aliquot using a ^{228}Ra-enriched spike after digestion, separation and purification according to the protocol given in Pelt et al. (2013) and adapted from previous works by Chabaux et al. (1994) and Ghaleb et al. (2004). Blanks ranged between 30 and 171 pg for U and 160 and 190 pg for Th and were < 0.1 fg for Ra and <1 ng for Sr; thus, the blanks were negligible compared to the Sr and U-Th-Ra amounts analyzed in the samples. The repeatability of the Sr, Th and U isotopic analyses was tested by repeated measurements of three solution standards, NBS 987, Th105 and HU1. The mean value of $^{87}Sr/^{86}Sr_{NBS987}$ was 0.71027 ± 0.00002 (n=22, 2SD (Standard Deviation)), that of $^{232}Th/^{230}Th_{Th105}$ was 217080 ± 2400 (n=37, 2SD) and $(^{234}U/^{238}U)_{HU1}$= 0.999 ± 0.004 (n=72, 2SD). In addition, repeated analyses of the AThO rock standard yielded a mean U activity ratio value of 1.000 ± 0.004 (n=10, 2SD) and a $^{232}Th/^{230}Th$ isotopic ratio of 182840 ± 1238 (n=6, 2SD). All these data are consistent within errors with previously published data (Pelt et al., 2013 and references therein). The ^{226}Ra concentration of the ^{228}Ra-spike was regularly calibrated against the AThO rock standard assuming secular equilibrium for the ^{226}Ra-^{230}Th isotopes. The analysis of the ($^{226}Ra/^{230}Th$) ratios of the BEN rock standard gives a value of 1.002 ± 0.017 (2SD) that is entirely consistent with the assumed secular equilibrium value (Pelt et al., 2013).

3.2. Vegetation samples

Each sample was first washed with deionized ultrapure water in an ultrasonic tank/bath to remove soil and airborne particles. The samples were then dried at 60°C until a constant mass was reached and finally crushed within a specific agate disk mill. Two aliquots of 2 to 10 g of plant material powder were digested on a hotplate in conventional PFA Teflon© beakers successively using a HNO_3-H_2O_2 mixture and HNO_3-HF (a) to determine $^{87}Sr/^{86}Sr$ isotopic ratios, U-Th concentrations and U-Th activity ratios using the same protocol as described above for the soil samples and (b) to determine ^{226}Ra concentrations. To avoid interference by Ca during TIMS measurements, excess Ca was removed from the

samples using a pretreatment based on manganese complexation according to a protocol adapted from Ghaleb et al. (2004). After complete sample mineralization, the residue was dissolved in 1 to 2 ml of 6N HCl bidistilled and 150 ml of ultrapure water. Approximately 150 µl of 0.5 N $KMnO_4$ was added to oxidize the residual organic matter. The solution was heated for 10 min at 80°C before adjusting the pH to 10-11 with 1 M NaOH. Next, 200 µl of 0.5 N $MnCl_2,4H_2O$ was added to initiate Mn-oxide precipitation, onto which Ra sorbed, while most Ca remained in solution. The mixture was heated at 110°C for 15 min, cooled and centrifuged at 4000 rpm for 10 min. The precipitate was washed with hot ultrapure water, centrifuged and dissolved in 5 to 10 ml of 6N HCl. After evaporation, the residue was dissolved with 2 N HCl to separate and purify the Ra fraction according to the protocol detailed above for rocks. All blank procedures ranged between 7 and 41 pg for U, 0.7 and 162 pg for Th, <0.04 fg for Ra and < 1 ng for Sr, which are negligible compared to the Sr and U-Th-Ra amounts analyzed in the samples.

3.3. Soil solutions, rainwaters and throughfalls

Water samples, i.e., soil solutions, rainwater and throughfalls, were filtered through a 0.45 µm cellulose acetate membrane filters in the laboratory a few hours after sampling. Each water sample was subdivided into two aliquots: one acidified with bidistilled 13.5 N HNO_3 to pH≈1 for trace element and isotopic analyses; another one, not acidified, for measurement of pH, conductivity, and for analysis of major element and dissolved organic carbon (DOC) concentrations following the standard procedures used in the laboratory (e.g., Lucas et al., 2010; Schaffhauser et al., 2014; Gangloff et al., 2014) and detailed in Prunier et al. (2015). Trace element concentrations were determined by ICP-MS with an uncertainty better than 10%. The precision and accuracy of the results were checked by regular analyses of the SLRS-4 riverine standard. For Sr isotopic analyses and U-Th-Ra disequilibria determination, between 10 and 2000 ml of water samples were used to reach 5 to 20 ng of U, 300 to 400 ng of Th, 100 ng of Sr and 2 to 40 fg of Ra, which are necessary for precise isotope determinations. Samples poor in U and Th were preconcentrated by coprecipitation with Fe hydroxide (Chabaux et al., 1995; 1997) or by total evaporation if the DOC concentration was too high. Blanks ranged

between 12 and 55 pg for U, 150 pg for Th, < 0.07 fg for Ra and < 1 ng for Sr. These quantities are negligible compared to those in the samples.

4. RESULTS

Major and trace element concentrations and the U and Sr isotope ratios were presented and discussed in Prunier et al. (2015). Therefore, the present work focuses on the U-Th-Ra isotope data, which, combined with Sr isotope ratios and major and trace element concentrations, allow for emphasizing the potential of using U-Th-Ra systematics in soils, soil solutions and trees to better constrain the sources and pathways of element transfers involved in the biogeochemical cycles in forest ecosystems. The main data used and discussed in this study are given in Table 1a-d. The complete dataset of the major and trace element concentrations, including REE concentrations, is provided in Supplementary Material Tables EA1-2-3.

4.1. Mineralogy

In line with previous works on the soils in the Strengbach catchment (Ficher et al., 1998a, 1998b; Aubert et al., 2001; Stille et al., 2009), Prunier et al. (2015) showed that the main minerals of bulk soil samples are quartz, feldspars (orthoclase and albite), muscovite and clay minerals. Biotite and traces of apatite were observed in both soil profiles, while hematite (< a few %) was detected by XRD in only the spruce soil profile. The 2 µm grain size fractions of the samples from the spruce and beech profiles were composed of kaolinite and illite, with interstratified illite-vermiculite and/or illite-smectite and traces of goethite, which were more abundant in the spruce samples than in the beech samples. The minor minerals detected by SEM were zircons, monazites and apatites.

The new SEM observations of the grain size fractions in the present study emphasized that some zircons have blunted or fractured surfaces, which could be evidence of weak surface weathering of zircons (Fig. EA1a). In addition, some Ba and Sr sulfates were observed in the 2-50 µm and 50-100 µm fractions of the VP 90-100 horizon (Fig. EA1b). SEM observations have also shown that the “so-called” <2 µm fraction of the HP90-100 horizon, used in Prunier et al. (2015), clearly encompasses much larger particles than expected, most likely due to separation problems. This fraction was therefore not considered in the present study.

330

331 **4-2: U and Th concentrations in grain size fractions**

332 As recognized by Prunier et al. (2015), the comparison of U concentrations with
333 major and trace elements in the different grain size fractions showed that the U
334 budget in these soils is strongly controlled by secondary minerals and minor
335 primary minerals such as phosphates. A more thorough comparison of the
336 variations in U and Th concentrations with major and trace element concentrations
337 in the different soil samples and grain size fractions allows for a better constraint of
338 the nature of the minor mineral phases controlling the U and Th budget in these
339 soils and their varied influences in the two plots and the different fractions. The
340 covariations between the U-Th concentrations and Zr concentrations (Fig. 2)
341 confirm that the U and Th budgets in the 2-50 μm and 50-100 μm grain size
342 fractions are at least partly controlled by zircons. In the beech (HP) plot samples, the
343 correlations between U, Th and Fe_2O_3 and P_2O_5 concentrations for the coarse grain
344 size fractions (Fig. 2) indicate that U and Th in the HP soils are also tightly
345 associated with phosphate and Fe-bearing phases. However, in the spruce (VP) plot
346 samples, U and Th concentrations were better correlated with Zr than with P
347 concentrations, suggesting that zircon is likely one of the main carriers of U and Th
348 in spruce plots but not in beech plots. The comparison of the Ba concentration with
349 the U and Th concentrations in the grain size fractions extracted from the different
350 soil horizons (Fig. EA2) indicates that some Ba-rich mineral phases also control the
351 U and Th budgets in the spruce soil horizons, especially in the 2-50 μm and 50-100
352 μm grain size fractions, while this control is much less present in the beech soil
353 horizons. Sulfate minerals, observed by SEM, and Ba-rich K-feldspars also observed
354 in Strengbach granitic rocks are among the possible Ba-carrying minerals, as well as
355 Mn oxyhydroxides (Palumbo et al., 2001, Vaniman et al., 2002, Ghaleb et al., 2004).
356 The VP spruce soil horizons had higher Ba levels than the HP soil horizons, implying
357 that the abundance of these Ba-rich minerals was low in the HP sites. This difference
358 can be related to the weak hydrothermal overprint of the bedrock from the southern
359 slope where the beech plot stands, which is thus likely less marked by hydrothermal
360 mineralizations that contain barites and oxyhydroxide minerals.

Together, these data emphasize the importance of secondary minerals as well as minor primary minerals (zircons, sulfates and phosphates minerals) in the U and Th budget in the soil of the two experimental plots in the Strengbach catchment.

4.3. Th isotopic ratios and U-Th-Ra disequilibrium in grain size fractions

The present data show important variations between the ($^{230}Th/^{232}Th$) ratios and U/Th chemical ratios in the different grain size fractions and between the different plots (Table 1a) with systematically lower values in the spruce (VP) than in the beech (HP) plots. The <2 μm fraction of the HP (30-40 cm) soil horizon shows the highest ($^{230}Th/^{232}Th$) ratio [($^{230}Th/^{232}Th$) = 4] of all the grain size fractions analyzed in this study, with a value close to that of apatite (≈5 from U/Th ratios given in Aubert et al., 2004; 2001) (Fig. 3). The 2-50 μm and 50-100 μm grain size fractions from the spruce site exhibit the lowest ($^{230}Th/^{232}Th$) ratio (0.71-0.75). The correlation between ($^{230}Th/^{232}Th$) and ($^{238}U/^{232}Th$) ratios and Zr concentrations observed for the VP grain size fractions (Fig. 4), as well as with Ba concentrations (Fig. 5), highlights the low U/Th and Th activity ratios of the zircons and the Ba-bearing minerals, which are much lower than the Th activity ratios of the other primary granite minerals (apatite, biotite, muscovite and albite) as estimated from the U/Th ratio given in Aubert et al. (2001; 2004). For the HP plot, all the grain size fractions, except the two 1.6-2 mm fractions, show a very good covariation between ($^{230}Th/^{232}Th$) and P_2O_5 contents (R=0.972) (Fig. 6).

The ^{238}U-^{234}U-^{230}Th-^{226}Ra data (Tab. 1a) show that all grain size fractions are marked by systematic ^{238}U-^{230}Th disequilibrium with ($^{238}U/^{230}Th$) <1. The comparison of the ^{238}U-^{234}U-^{230}Th-^{226}Ra disequilibria in the different grain size fractions indicates the higher ($^{234}U/^{238}U$) and ($^{230}Th/^{234}U$) ratios in the beech plot grain size fractions than in the spruce plot as well as the higher ratios for a given plot in the < 2 μm fractions than in the other fractions (Fig. 7a,b). This systematic disequilibrium is, however, not observed for the ^{226}Ra-^{230}Th disequilibria. With the exception of the two <2 μm fractions from the VP plot, which are marked by relatively high ($^{226}Ra/^{230}Th$) ratios (1.42, 1.6), all other grain size fractions show rather similar ($^{226}Ra/^{230}Th$) ratios scattering between 0.88 and 1.13 (Fig. 7b) that are unrelated to the size of the fractions or the depth of the analyzed horizons. At the scale of the spruce plot, however, the ($^{226}Ra/^{230}Th$) and ($^{230}Th/^{234}U$) ratios

decrease in the following order: <2 μm fraction, 2-50 μm fraction and other fractions. For the beech plots, such a systematic disequilibrium is not apparent for the ($^{226}Ra/^{230}Th$) ratio, but it is still observed for the ($^{230}Th/^{234}U$) ratio.

4.4. U-Th-Ra and Ba in soil solutions

As for the grain size fractions, and as already noted in Prunier et al. (2015), the soil solution data point to significant geochemical differences between the soil solutions collected at the two experimental plots in both major and trace element concentrations. The soil solutions from the VP spruce plot have higher TDS and conductivities and lower pH values than those from the HP beech plot. The soil solutions from the VP spruce plot are also 5 to 10 times richer in Mg, K and Ca than those from the HP plot (data in supplementary materials Tab EA3). Our data show that such differences are also seen in the U-Th-Ra systematics and that Ba has a distinct comportment compared to Sr and Ca elements.

- Alkaline-earth elements

The trace element concentrations of the soil solutions show higher alkaline-earth (Sr, Ba) concentrations under spruces than under beeches (Fig. EA3). Within a plot, the Ca and Sr concentrations are higher in the surface soil solutions than in the deep layers, which is certainly related to root absorption of these elements by the trees, as evidenced by Ca isotopes (Cenki-Tock et al., 2009; Schmitt et al., 2017). Compared to Sr and Ca, Ba shows different behavior in the spruce plot (Fig. EA3), where the highest Ba concentrations are observed for soil solutions from 30 cm depth, with a negative correlation with the sulfate contents (Fig. EA3). A negative correlation is also observed for the -60 cm soil solution data but with a different slope (Fig. EA3). The observation that positive, linear correlations passing through the origin can be defined between the Ba and $1/SO_4$ concentrations for these two soil solutions (Fig. EA3) likely indicates $BaSO_4$ saturation, meaning that the Ba and SO_4 concentrations at depths of 30 cm and 60 cm are controlled by the precipitation of $BaSO_4$. The SEM observation of Ba sulfate precipitates in soil solutions collected at depths of 30 cm and 60 cm supports this interpretation (Fig. EA1c). The atypical Ba concentrations of the 30 cm soil solutions are clearly evidenced in a Ba vs Mg concentration diagram, which indicates a specific source of Ba at this depth, but not

at 60 cm. The positive trend between the K and Ba concentrations in 30 cm soil solutions likely suggests that the Ba input in these soil solutions results from the dissolution of Ba-rich K-feldspars, at a sufficiently high level to cause a BaSO4 precipitation. For the 60 cm soil solutions, the correlation between Mn and Ba (Fig. EA3) suggests the dissolution of other minerals, such as Mn oxides and likely sulfates, which are often associated with Mn oxides in hydrothermal veins intersecting granitic rocks. The dissolution of sulfate minerals can thus control the $BaSO_4$ saturation of the 60 cm soil solutions. Such a dissolution at 60cm depth and not a 30cm depth can also account for the observation of a correlation between the Sr and $1/SO_4^{2-}$ concentrations in only the 60 cm depth soil solutions (Fig. EA_3), suggesting that the supply of sulfate is sufficient to also cause the saturation of $SrSO_4$ in these waters or also of $(SrBa)SO_4$. Furthermore, dissolution of SO_4^{2-} bearing mineral phases at 60 cm depth readily explains why the soil solutions from 60 cm depth at the spruce plot are the only water reservoir in the Strengbach catchment whose SO_4^{2-} concentrations did not decrease from 1990-2010 (Fig. EA_4 and Ackerer et al., 2018).

- Th activity ratios and U-Th-Ra systematics

The ($^{230}Th/^{232}Th$) ratios of the (HP) beech plot soil solutions are significantly higher than those of the (VP) spruce plot and those of most of the corresponding grain size fractions (Fig. 3). Only the <2 μm grain size fraction of the HP (30-40 cm) soil layer and apatite had higher ($^{230}Th/^{232}Th$) ratios. Compared to the grain size fractions and the granite-derived primary minerals, the soil solutions of the beech plot exhibit relatively high Th isotope ratios, namely, ($^{230}Th/^{232}Th$) of 4 and 3.7 for the HP-10 cm and HP-70 cm soil solutions, respectively. These ratios are close to the ($^{230}Th/^{232}Th$) of the <2 μm fraction but with different U/Th ratios depending on their depth of collection. In the ($^{230}Th/^{232}Th$) vs. ($^{238}U/^{232}Th$) diagram (the so-called isochron diagram), the surface solution (-10 cm) plot is relatively close to the <2 μm grain size fraction, while the deep solution plot is much closer to the equiline (1:1 line in the isochron diagram) (Fig. 3). In the spruce plot, the Th activity ratios were analyzed in the soil solutions from the depths of only -5 cm and -10 cm due to the very low Th concentrations in the deeper soil solutions. As apparent in Fig. 3, these soil solutions have very similar ($^{230}Th/^{232}Th$) (1.6) but relatively scattered

460 ($^{238}U/^{232}Th$) ratios (0.7-1.04). The Th activity ratios in these solutions are higher
461 than those analyzed in the corresponding grain size fractions.
462 Based on the available ($^{226}Ra/^{230}Th$) ratios in both the beech and spruce plots, the
463 soil solutions have higher ($^{226}Ra/^{230}Th$) ratios than the corresponding soil fractions
464 (Table 1a-b). Furthermore, in the ($^{226}Ra/^{238}U$) vs ($^{234}U/^{238}U$) diagram (Fig. 8a), the
465 (VP) spruce plot soil solutions from depths of 10 cm, 30 cm and 60 cm define a
466 positive correlation with the lowest ($^{226}Ra/^{238}U$) ratios in the 30 cm soil solutions.
467 Moreover, the <2 μm and 2-50 μm grain size fractions from the VP 30-40 cm soil
468 horizon are aligned together with the soil solution collected from a depth of 30 cm
469 (Fig. 8b).
470
471 **4.5. Geochemical and isotopic characteristics of the vegetation samples.**
472 The geochemical and isotopic data of the vegetation samples are given in Table 1c.
473 These data show concentration variations, which vary from one tree to another and
474 within a tree between its different compartments. Uranium and Th concentrations
475 are higher in the roots than in the aerial parts of trees, which is not the case for Ba
476 and ^{226}Ra. This may indicate a possible fixation of U and Th on roots without real
477 transport within the aerial parts of trees at the difference of Ba and Ra. Compared to
478 soil solutions, soil samples and grain size fractions, trees are enriched in Ca, Sr, Rb
479 and K, as well as in Ba (Table 1). The data also point to high variability in the relative
480 concentrations of these elements between the different parts of the trees, even for
481 the elements from the same chemical family, such as the alkaline-earth Ca, Sr, Ba.
482 The Ca/Sr and Ba/Sr ratios vary by a factor of 5 or more in the beech trees and by a
483 factor of 10 in spruce. Compared to U and Th, Ra is also highly enriched in the trees,
484 with ($^{226}Ra/^{230}Th$) ratios as high as 5 and ($^{226}Ra/^{238}U$) ratios ranging from 1.12 up
485 to 79 in spruce. In beech, ($^{226}Ra/^{238}U$) ratios range from 21.5 to 1413, and
486 ($^{226}Ra/^{230}Th$) ratios range from 19.8 to 164.4.
487 The vegetation samples show $^{87}Sr/^{86}Sr$ isotope ratios similar to those of the
488 corresponding soil solutions (Fig. 9). As noted in Prunier et al. (2015), the
489 ($^{234}U/^{238}U$) ratios of the beech samples are similar to those of the corresponding soil
490 solutions and soil samples, while they are systematically higher in the vegetation
491 samples from the spruce plot, with ($^{234}U/^{238}U$) ratios ≥ 1 in spruce samples for
492 ($^{234}U/^{238}U$) ratios ≤1 in the soil solution samples (Fig. 10, and Prunier et al., 2015).

493 The beech and spruce samples have ($^{238}U/^{230}Th$) ratios close to equilibrium
494 [($^{230}Th/^{238}U$)≈1] and hence plot along the equiline in the isochron diagram, with
495 ($^{230}Th/^{232}Th$) ratios ranging between 1 and 1.4 for beech and close to 1 for spruce,
496 which is very different from those of the corresponding soil solutions (Fig. 3).
497
498 **5. DISCUSSION**
499
500 ***5-1 U-Th-Ra fractionation by vegetation***
501 The comparison of the vegetation chemical data with the soil and soil solution data
502 points to an important enrichment of Ba and ^{226}Ra relative to U and Th in trees,
503 which suggests that trees can have a much greater impact on the Ra (Ba) budget
504 than the U and Th budgets in forest ecosystems. This impact is made clear when the
505 uptake of U, Th, Ba, Ra by tree roots and their respective recycling through litter
506 degradation are compared with their drainage by soil solutions (Tab. 2a,b). The
507 uptake fluxes can be estimated using the Ca uptake fluxes given in Poszwa et al.
508 (2000) for the Strengbach beeches and spruces and the U/Ca, Th/Ca, Ba/Ca and
509 $^{226}Ra/Ca$ ratios measured in the present study in the different tree organs (Tab.2a).
510 These chemical ratios can vary within a tree, such as Ca/Sr ratios (e.g., Poszwa et al.
511 2000; 2003; Wiegand et al., 2005; Blum et al., 2008; Drouet et Herbauts 2008),
512 leading to a relatively large uncertainty in the calculated uptake fluxes. However, the
513 data clearly indicate that the U and Th uptake fluxes are low compared to the
514 drainage by soil solutions (Tab. 2b), while they are comparable for Ba and Ra.
515 Similarly, the comparison of the maximum calculated U and Th fluxes coming from
516 litter degradation with those drained by the soil solutions demonstrates the very
517 low contribution of litter degradation on the U and Th budgets of soil solutions,
518 which is not the case for Ba and Ra (Tab. 2b). These results demonstrate that Ra and
519 Ba are highly cycled by vegetation, which is the opposite for U and Th, and that root
520 uptake and litter degradation can be important actors in Ra-Th and Ra-U
521 fractionation in soils and soil solutions (see also Rihs et al., 2011). This result is
522 clearly illustrated by the U-Th-Ra disequilibria variations in the soil solutions of the
523 beech plot at 10 cm depth (Fig. 11). The distribution of the data points in the
524 ($^{230}Th/^{234}U$) vs ($^{226}Ra/^{230}Th$) diagram indicates a more important Ra contribution
525 from litter decay to the soil solution in March 2005 than in May 2006, which mainly

impacts the ($^{226}Ra/^{230}Th$) ratios of the soil solutions and has much less of an impact on the ($^{230}Th/^{234}U$) ratios. The data also show that this type of vegetation impact is visible at 10 cm depth but is not visible at 70 cm depth, which indicates that tree-related fractionation is confined to superficial soil and soil solutions. The ^{238}U-Ba-^{226}Ra data of soil solutions under spruces supports this conclusion. For the spruce plot, the soil solution data collected at 10, 30 and 60 cm and the data from the <2 µm and 2-50 µm grain size fractions of the 30-40 cm soil horizon define two linear trends that converge towards the values of the 30 cm soil solutions in the ($^{238}U/^{226}Ra$) vs ($^{234}U/^{238}U$) diagram (Fig. 7a). The latter soil solutions have the lowest ($^{234}U/^{238}U$) and ($^{226}Ra/^{238}U$) ratios measured at the site (<1), which cannot be explained by the contributions of U and Ra fluxes from vegetation recycling, as all vegetation samples are marked by ($^{226}Ra/^{238}U$) >>1. Based on the ^{238}U-^{234}U-^{226}Ra-Ba systematics, it is also difficult to invoke a variable vegetation contribution from one soil solution sample to another to explain the ($^{226}Ra/^{238}U$) and ($^{234}U/^{238}U$) differences among the soil solutions from depths of 30 cm and 60 cm. If this would have been the case, a correlation between the Ba/U and ($^{226}Ra/^{238}U$) ratios of these soil solutions should have been observed, which is not the case (Fig. 7b). Thus, the geochemical end-member with ($^{234}U/^{238}U$) and ($^{226}Ra/^{238}U$) ratios <1 likely represents a weathering end-member resulting from the destabilization of secondary minerals contained in the finest grain size fractions of the 30-40 cm soil horizon. The covariations observed in the ($^{226}Ra/^{238}U$) vs ($^{234}U/^{238}U$) and ($^{226}Ra/^{238}U$) vs Ba/U diagrams between the 30 and 60 cm soil solutions (Fig. 7a, b) likely reflect the control by different mineral fractions in each of these soil solutions. For the 30 cm soil solution, a high contribution of a mineral fraction with high Ba/U ratios but depleted in ^{234}U and ^{226}Ra relative to ^{238}U was observed. This mineral fraction likely explains the low ($^{234}U/^{238}U$) and ($^{226}Ra/^{238}U$) ratios of the 2-50 µm fractions of the 30-40 cm soil horizon. The 2-50 µm fractions of the 30-40 cm soil horizon are the most Ba enriched. Thus, mobilization of weathering products of Ba-rich phases, such as Ba-rich K-feldspar evidenced in § 4-4, likely controls the U-Ba-Ra characteristics of the 30 cm deep soil solutions. For the 60 cm deep soil solutions, other minerals or less contribution of these Ba-rich minerals must be invoked to explain their U-Ra-Ba characteristics, which is consistent with the proposition for

these soil solutions of a specific weathering flux from oxides and sulfate minerals (see section 4-4).

However, regardless of the precise origin of weathering fluxes explaining the U, Ba, Ra systematics within the deep soil solutions of the spruce plots, the results clearly show that the impact of vegetation on U-(Th)-Ba and -Ra fractionations is visible mainly in the surface soil horizons and soil solutions and much less in the deeper ones. This conclusion is consistent with the demonstration that the ($^{226}Ra/^{230}Th$) ratios in the shallowest soil layers can be affected by vegetation changes/types over short timescales (Rihs et al., 2016). Moreover, this conclusion supports the assumption of Ackerer et al. (2016) and the suggestions of Gontier et al. (2015) and Rihs et al. (2016) that the deeper part of the weathering profiles below the zone of vegetation influence is certainly the most adapted zone to apply the U-series nuclides methodology classically developed for recovering regolith production rates (e.g., Dequincey et al., 2002; Dosseto et al., 2008; Chabaux et al., 2013). The highly contrasted behaviors of Ra and U-Th regarding vegetation cycling also has implications for the interest in these elements and their isotopic ratios for tracing biogeochemical cycles and water-rock interactions in forest ecosystems. Thus, being highly absorbed by trees, Ra and its isotopic ratio ($^{228}Ra/^{226}Ra$) should become a useful tracer of the impacts of vegetation on the geochemical cycles in the biosphere. Moreover, the very different half-lives of ^{228}Ra (5.75 a) and ^{226}Ra (1600 a) should make Ra also a potential chronometer of the litter degradation rate, in addition to being relevant for constraining the chemical element residence time in the vegetation (e.g., Baeza et al., 1999). The second important implication of the results is linked to the small impact of vegetation cycling on the U and Th budgets in soils and soil solutions. These elements are therefore mostly controlled by water-rock interactions. This finding is certainly the main difference between these isotopic ratios and $^{87}Sr/^{86}Sr$ or $^{143}Nd/^{144}Nd$, as Sr and Nd are two significantly biocycled chemical elements (e.g., Stille et al., 2006; 2009). The Sr and Nd isotopic ratios in soils and soil solutions thus represent an integration of lithogenic fluxes directly derived from water-rock interactions with recycled and hence “delayed” fluxes due to Sr and Nd vegetation cycling. Uranium and thorium are probably among the few geochemical elements to be controlled by only direct water-rock

591 interactions and therefore to be specific tracers of these interactions. The
592 combination of this property with (a) the large range of the variations in the
593 ($^{230}Th/^{232}Th$) ratios in the soil minerals, especially in secondary and minor minerals
594 (this study; Bosia et al., 2016; 2018) and (b) the low contributions of rainwater and
595 atmospheric deposits on U and Th soil and soil solution budgets on granitic lithology
596 (e.g., Chabaux et al., 2005; 2013) indicates that the Th activity ratio has the potential
597 to become a powerful tracer of the sources of the chemical fluxes in the soils, soil
598 solutions and vegetation. Such an interest is illustrated in the following two sections.
599

600 **5-2 U-Th tracing weathering fluxes in soil solutions**

601 Previous studies have shown that Sr and Nd isotopes in soil solutions and streamlets
602 in the Strengbach watershed principally result from apatite and feldspar dissolution
603 (Aubert et al., 2001, Stille et al., 2006, 2009). The proximity of the soil solution HP-
604 70 (beech plot) to the ($^{230}Th/^{232}Th$-$^{238}U/^{232}Th$) equiline between the apatite and the
605 feldspars data points (Fig. 3) is consistent with this interpretation. The soil solution
606 HP-10, however, clearly suggests a contribution of a third flux in addition to the two
607 previous fluxes with a U-Th signature close to that of the <2 μm grain size fraction,
608 which is also true when looking at the data in the ($^{230}Th/^{232}Th$) vs $^{87}Sr/^{86}Sr$ diagram
609 (Fig. 12).

610 The covariation between ($^{230}Th/^{232}Th$) and P_2O_5 contents in the grain size fractions
611 of the beech plot samples (Fig. 6) implies that Th isotopes are essentially controlled
612 by the presence of phosphate minerals with high Th activity ratios. Therefore, the
613 high Th activity ratios of the <2 μm fraction are imposed by phosphate minerals,
614 which in turn are those that controlled the U-Th-Sr weathering fluxes from the <2
615 μm fractions. As in the grain size fractions of the beech plot, the P_2O_5 contents do
616 not correlate with the corresponding Ca contents (not shown), it is not apatite but
617 probably other phosphate-rich, apatite replacement phases that control the
618 covariation between P_2O_5 contents and the ($^{230}Th/^{232}Th$) ratios in such a system.
619 Furthermore, as the ($^{238}U/^{232}Th$) ratio of the <2 μm grain size fraction from the HP
620 plot (<1.48) is significantly lower than that of apatite (5.07) and has relatively low
621 Sr concentrations relative to Fe, the formation of such secondary minerals from the
622 dissolution of apatite during weathering caused mobilization of not only Ca (Stille et
623 al., 2009) but also apparently apatite-derived-U and Sr (Fig. EA2). Such a difference

624 in the mobilization of U-Th-Sr during the weathering of apatite and formation of
625 secondary phosphate phases readily explains why the $^{87}Sr/^{86}Sr$ ratio (0.85) of the
626 <2 μm grain size fraction from the HP plot (30-40 cm) is significantly higher than
627 that of primary apatite (0.716), while the ($^{230}Th/^{232}Th$) ratio of this fraction (4.085)
628 remains close to that of apatite (5).
629 Altogether, these data indicate that in the beech plot, the dissolution of secondary
630 phosphates in the <2 μm fraction controls an important part of the U-Th-Sr chemical
631 budget of the surface soil solutions. These secondary minerals and their U-Th-Sr
632 isotopic signatures must therefore be inherited from a weathering process anterior
633 to the process controlling the present-day U-Th-Sr isotopic signature of the surface
634 soil solutions. Based on these data, a two-step weathering scenario can thus be
635 proposed for the beech plot: (a) predominant dissolution of primary minerals in the
636 deep soil horizons and the formation of secondary minerals partially maintain the
637 isotopic signature of the weathered primary minerals; (b) dissolution of these
638 secondary minerals, in particular those contained in the finest grain size fractions, in
639 the surface soil horizons. Schmitt et al. (2017) showed that the Sr isotope ratios of
640 the soil solutions increased from 2006 to 2011 in the beech plot at 10 cm depth but
641 not at 70 cm depth, which indicates that the contribution of the secondary minerals
642 to the chemical budget of the surface soil solution increased over this period and
643 hence could be a relatively recent process. This result is consistent with the results
644 of Rihs et al. (2011), who concluded based on short half-lived radionuclides of the
645 ^{232}Th-series that the surface soils under the beech plot have been affected by recent
646 (<30a) weathering processes.
647 For the spruce (VP) plot, the scattering of the 5 cm and 10 cm deep soil solution data
648 in the isochron diagram (Fig. 3), i.e., similar ($^{230}Th/^{232}Th$) ratios but variable
649 ($^{238}U/^{232}Th$) ratios, cannot be explained by the varying tree contributions to the U-
650 Th budget of the different soil solutions, as tree samples are marked by
651 ($^{230}Th/^{232}Th$) ratios lower than those measured in the surface soil solutions. For this
652 reason, and in line with the low contribution of tree cycling to the U and Th budget,
653 it is proposed that the U-Th budget of the spruce surface soil solutions (VP plot) is
654 controlled, as occurs in the beech plot, by a mixture of U-Th coming from the
655 dissolution of secondary minerals with ($^{230}Th/^{238}U$)<1 and high ($^{230}Th/^{232}Th$) ratios
656 and more “equilibrated” U-Th coming from the dissolution of primary minerals.

However, unlike the beech plot, none of the analyzed grain size fractions in the spruce plot show U-Th signatures similar to that of the surface soil solutions. In particular, all of the grain size fractions have much lower ($^{230}Th/^{232}Th$) ratios than those in the solutions, which can be explained in two ways. First, the U-Th signature of the 30-40 cm grain size fractions are not representative of the 10 and 5 cm deep fractions because of the local lithological heterogeneities (cf section 4-4). Second, the weathering processes in the spruce plot were initially similar to those in the HP plot, but this plot is now in a much more advanced weathering stage. Thus, it can now be proposed that a large part of the minerals carrying the apatite signature has been leached much more intensively under spruce than under beech, causing an important loss of these minerals and hence a significant decrease in the ($^{230}Th/^{232}Th$) ratios of the grain size fractions. This scenario, which is favored by the more acidic conditions under the spruce plot, is also supported by the observation of an earlier increase in the Sr isotopic ratios in the soil solutions of the VP spruce plot than that in the HP beech plot: between 1997 and 2006 for the spruce plot (Prunier et al., 2015) and between 2006 and 2011 for the beech plot (Schmitt et al., 2017) (Fig. 9).

Thus, based on these results, the weathering scenario retained for the spruce plot (VP) is similar to that invoked for the beech plot (HP) but with a slightly different mineralogical composition and a much more advanced degree of alteration of the fine grain size fractions of the VP surface soil horizons. This scenario, which is also consistent with the B isotope data in the Strengbach catchment (Lemarchand et al. 2012), not only accounts for the earlier modification of the Sr isotope ratios in the soil solutions of the spruce plot but also explains why the <2 μm and 2-50 μm fractions are more depleted in Sr, Ca, U, Th and REE (Fig. EA2) for equivalent Fe contents in the spruce (VP) than in the beech (HP) plot. This scenario is also consistent with the weathering indexes calculated in Prunier (2008) following the approaches proposed in Kronberg and Nesbeitt (1981). Such a difference between the degree and timing of the destabilization of the beech and spruce plots is likely the consequence of a larger chemical export by soil solutions under the spruce than the beech plot. Climatic differences exist between the two slopes (e.g., Viville et al., 1993; 2012), with longer and more intense sunshine duration on the VP south-facing slope, which may explain part of this difference. But, this difference is also

690 certainly related to the difference in the pH of the soil solutions under these two
691 plots, which is clearly linked to the differences in vegetation cover. The more acidic
692 soil solutions under spruces allowed for stronger leaching of the soils in the spruce
693 (VP) plot than allowed by the less acidic soils in the beech (HP) plot. The fast-
694 growing spruces found in the VP plot were planted for forest exploitation. These
695 trees generally induce both a strong acidification of soils and soil solutions via the
696 decomposition of the needles and a high nutrient export flux that is much greater
697 than that induced by trees naturally growing on the site (fir - beech) (e.g., Binkley
698 and Valentine, 1991; Alriksson and Eriksson, 1998; Augusto et al., 2015; Berger et
699 al., 2009; Cremer and Prietzel, 2017). The cause of soil depletion and irreversible
700 modification of the tree nutrient carrier phases by vegetation have not been
701 sufficiently considered until now. The vegetation could play an important role and
702 may be equivalent or even more important than the effects of acid rain. For the
703 Strengbach catchment, we propose that the artificial change in vegetation explains
704 much of the differences in soil destabilization states between the beech and spruce
705 plots.
706
707 **5-3 U-Th, tracing the source of elements in the water-tree system.**
708 The Sr-U-Th isotopic characteristics of soil solutions and trees are different. Soil
709 solutions have Sr isotopic ratios that are relatively close to those of trees, which is
710 consistent with the biorecycled behavior of Sr. Nevertheless, Sr isotopic ratios in
711 trees are systematically slightly less radiogenic than those in soil solutions (Fig. 9).
712 The difference between soil solutions and trees is more marked in the spruce plot
713 than in the beech plot and increases with time (Fig. 9). As discussed in the previous
714 section (§ 5.2), this difference might be related to the higher or lower degree of
715 modifications of the water-rock-vegetation system in these two plots, as the
716 alteration processes have been more intensively modified in the spruce (VP) plot
717 than in the beech (HP) plot. This difference may also point to the occurrence of Sr
718 fluxes in soil solutions, which are different from those taken up by the tree and,
719 therefore, different from those recycled by vegetation. The observations that the U
720 activity ratios are higher in trees than in soil solutions in the spruce (VP) plot and
721 that the Th ratios are systematically different between trees and soil solutions in
722 both plots support such an interpretation (Fig. 13). The beech plot soil solutions are

entirely consistent with the three-end-member mixing model proposed in the previous sections, between (1) the <2 μm grain size fractions marked by a high ($^{230}Th/^{232}Th$) ratio and a strong ^{234}U-^{238}U disequilibrium, (2) an apatite end-member with a high Th activity ratio and ^{238}U-^{234}U equilibrium and (3) a third end-member marked by a low ($^{230}Th/^{232}Th$) ratio and a ($^{234}U/^{238}U$) ratio close to equilibrium. However, the very contrasted values of soil solutions and tree samples indicate that beech trees absorb U and Th and probably also other nutrients not directly from the gravitational soil solutions collected in this study but from other reservoirs marked by different chemical and isotopic compositions, i.e. water-reservoir - like bounded waters, or possibly also directly from solids, as trees can uptake nutrients from solids without going through soil solutions (in Morgan and Connolly, 2013). The relatively low ($^{230}Th/^{232}Th$) ratios of trees can be derived from primary minerals, most likely biotite but also possibly apatite or feldspar, to account for the scattering of the Th activity ratios in the beech trees. The ^{234}U-^{238}U disequilibria in the tree samples are consistent with an uptake of U enriched in ^{234}U (by alpha recoil) from primary minerals. The absence of ^{238}U-^{230}Th fractionation suggests that during nutrient uptake, U and Th are not significantly fractionated. This conclusion of different U and Th sources for vegetation and soil solutions has also to be proposed for the spruce plot on the basis of the ($^{230}Th/^{232}Th$) vs ($^{234}U/^{238}U$) and vs $^{87}Sr/^{86}Sr$ diagrams (Fig. 13 and Fig. 12). In the ($^{230}Th/^{232}Th$) vs ($^{234}U/^{238}U$) diagram, the spruce plot soil solutions confirm the suggestion (§ 5-2) that the U-Th budget of spruce soil solutions is controlled by minerals with ($^{234}U/^{238}U$) <1 and low ($^{230}Th/^{232}Th$) ratios, i.e., the U-Th characteristics of Ba-rich and Zr-rich minerals in the spruce soils. On the other hand, spruce data in the ($^{230}Th/^{232}Th$) vs ($^{234}U/^{238}U$) diagram suggest that the U and Th sources for spruces might not be very different from those for beech, confirming that these trees absorb nutrients from a distinct reservoir to that controlling the U-Th budget in solutions collected by zero-tension lysimetric plates. The Strengbach results thus underscore an interest, certainly not anticipated so far, of the use of the U-Th systematics in the critical zone to constrain the nutrient source of the plants.

CONCLUSIONS

^{238}U-^{234}U-^{230}Th-^{226}Ra nuclide data and ($^{230}Th/^{232}Th$) ratios of soil minerals, soil solutions and trees from the two instrumented spruce and beech plots of the Strengbach catchment, yield new constraints on the sources and transfer pathways of these elements within the plant-soil-water system. It has ben demonstrated that these are clearly important geochemical parameters for tracing biogeochemical processes in the critical zone.

The results highlight the highly contrasting impact of trees on U-Th and Ra (Ba) budgets in forest ecosystems with Ra-Ba being highly and U-Th only slightly cycled by vegetation. Thus, tree uptake and litter decay can be a cause of Th-Ra(Ba) fractionations in soil solutions and soils, especially in the surface soil horizons. In contrast these processes have much less impact on U-Th fractionation, which is mainly controlled by water-rock interaction. Therefore, due to the strong cycling by trees, Ra together with its ($^{228}Ra/^{226}Ra$) isotopic ratio might become a powerful tracer and chronometer of the biogeochemical cycles in forest ecosystems and the processes they involve. On the other hand, due to the small impact of vegetation on the U and Th budget in soils and soil solutions, U and Th isotopes are probably among the few tracers to be specific indicators of water-rock interactions in the CZ markedly contrasting with classical isotope systems such as Sr or Nd, routinely used in the study of the CZ and significantly affected by vegetation cycling. Therefore, the characteristics of Th along with its fairly large range of activity ratios in soil minerals, especially in secondary and minor mineral phases, makes it a powerful and specific tracer of the sources of chemical fluxes in soils, soil solutions and vegetation. The Strengbach data emphasize this point but also highlight the utility of combining analysis of U, Th activity and Sr isotope ratios to constrain the source of these elements in soils and soil solutions. This approach places new constraints on the weathering processes affecting the Strengbach bedrocks and the nature and evolution of the reservoirs involved in (nutrient) element transfer at the plant-soil-water interface. It has been shown that minor mineral phases such as zircons, sulfates and phosphates significantly control the U and Th chemical budget and Th activity ratios of the soil samples and also the U-Th fluxes transiting in the soil solutions. The comparison of the U-Th-Sr isotopic characteristics of soil solutions and soil grain size fractions also allows the recognition of two stages of weathering with (a) dissolution of primary minerals and formation of secondary ones in the

788 deep soil horizons and soil solutions and (b) dissolutions of both primary and
789 secondary mineral phases in the finest soil grain size fractions of the nearest surface
790 soil horizons. The latter process might be related to recent modifications of
791 weathering in the catchment which is stronger and older under the spruce
792 compared to the beech plot. We propose that the artificial change in vegetation over
793 the past decades through planting of spruces significantly contributed to the current
794 differences in soil weathering between the beech and spruce plots. Spruce
795 plantation in the Strengbach catchment increased soil acidity, which accelerated
796 weathering of some minerals and likely also increased Ca leaching and the depletion
797 of the nutrient pool in the Ca-poor soil-vegetation system of the Strengbach
798 catchment. The U-Th-Sr results of this study point to the occurrence of isotopically
799 different reservoirs of these elements for trees and gravity soil solutions collected
800 by lysimetric plates. This further suggests that, in the case of the Strengbach
801 watershed, the gravity soil solutions cannot be the main, or even an important, tree
802 nutrient reservoir, which emphasizes that the U-Th systematics in the critical zone
803 can offer useful constraints on the nutrient source of the plants.
804
805
806 **Acknowledgments:** The study benefited from funding from the "Région Alsace"
807 (France), the CPER 2003-2013 "REALISE", and the "PPF REALISE" (University of
808 Strasbourg, France). During the course of the study J. Prunier benefited from the
809 funding of a Ph.D. scholarship from the University of Strasbourg. D. Million and R.
810 Boutin are thanked for the analysis of the major and trace element concentrations.
811 The corresponding author thanks very much the Associate Editor Frank McDermott
812 and two anonymous reviewers for their very constructive comments that have
813 helped us to highlight much better the main results and conclusions of this study. He
814 also thanks Robert Ellam for the discussions on the last version of the manuscript.
815

References:

Ackerer J., Chabaux F., Van der Woerd J., Viville D., Pelt E., Kali E., Lerouge C., Ackerer P., Di Chiara R., Négrel P. (2016). Regolith evolution on the millennial timescale from combined U-Th-Ra isotopes and in situ cosmogenic ^{10}Be analysis in a weathering profile (Strengbach catchment, France). Earth and Planetary Science Letters, 453, 33–43

Ackerer J., Chabaux F., Lucas Y., Clément A., Fritz B., Beaulieu E., Viville D., Pierret M.C., Gangloff S., Négrel Ph. (2018). Monitoring and reactive-transport modeling of the spatial and temporal variations of the Strengbach spring hydrochemistry. Geochemica Cosmochemica Acta, 225, 17-35.

Akerman, A., Poitrasson, F., Oliva, P., Audry, S., Prunier, J., 2014. Isotopic fingerprint of Fe cycling in an equatorial soil-1 plant–water system: The Nsimi watershed, South Cameroon. Chem. Geol. 385, 104–116.

Alriksson A. and Eriksson H.M., 1998. Variations in mineral nutrient and C distribution in the soil and vegetation compartments of five temperate tree species in NE Sweden. Forest Ecology and Management 108, 261-273.

Aubert D., Probst A., Stille P., and Viville D. (2002) Evidence of hydrological control of Sr behavior in stream water (Strengbach catchment, Vosges mountains, France. Appl. Geochem. 17, 285-300.

Aubert D., Stille P., and Probst A. (2001) REE fractionation during granite weathering and removal by waters and suspended loads: Sr and Nd isotopic evidence. Geochim. Cosmochim. Acta 65, 387-406.

Aubert D., Probst A., Stille P. (2004) Distribution and origin of major and trace elements (particulary REE, U and Th) into labile and residual phases in an acid soil profile (Vosges Mountains, France). Applied Geochem., 2004, 19, 6, p. 899-916. doi:10.1016/j.apgeochem.2003.11.005

Augusto L., De Schrijver A., Vesterdal L., Smolander A., Prescott C., Ranger J. 2015. Influences of evergreen gymnosperm and deciduous angiosperm tree species on the functioning of temperate and boreal forests. Biological Reviews, 90 (2) 444-466

Babcsányi, I., Imfeld, G., Granet, M., Chabaux, F. (2014) Copper stable isotopes to trace copper behavior in wetland systems Environmental Science and Technology,48, 5520-5529.

Babcsányi, I., Chabaux, F., Granet, M., Meite, F., Payraudeau, S., Duplay, J., Imfeld, I. (2016) Copper in soil fractions and runoff in a vineyard catchment: Insights from copper stable isotopes. Science of the Total Environment 557–558, 154–162.

Baeza A., Barandica J., Paniagua J.M., Rufo M., Sterling A., 1999. Using (^{226}Ra/^{228}Ra) disequilibrium to determine the residence half-lives of radium in vegetation compartiments. Journal of Environmental Radioactivity 43 (3): 291-304

Bagard M-L, Chabaux F, Pokrovsky O. S., Viers J., Prokushkin A. S., Stille P., Rihs S., Schmitt A.-D., Dupré B. (2011). Seasonal variability of element fluxes in two

858 Central Siberian rivers draining high latitude permafrost dominated areas
859 Geochimica Cosmochimica Acta, 75, 3335-3357.
860 Banwart, S.A. , Bernasconi, S.M., Blum, W.E.H., de Souza, D.M., Chabaux, F., Duffy, C.,
861 Kercheva, M., Krám, P., Lair, G.J., Lundin, L., Menon, M., Nikolaidis, N., Novak, M.,
862 Panagos, P., Ragnarsdottir, K.V., Robinson, D.A., Rousseva, S., de Ruiter, P., van
863 Gaans, P., Weng, L., White, T., Zhang, B. (2017) Soil Functions in Earth's Critical
864 Zone: Key Results and Conclusions. Advances in Agronomy 142, 1-27 DOI:
865 10.1016/bs.agron.2016.11.001
866 Banwart S.A., Nikolaos P. Nikolaidis N.P., Zhu Y-G, Peacock C.L., Sparks D.L. (2019)
867 Soil Functions: Connecting Earth's Critical Zone. Annu. Rev. Earth Planet. Sci.
868 47:333–59.
869 Beaulieu E., Lucas Y., Viville D., Chabaux F., Ackerer P., Goddéris Y., Pierret M.C.,
870 Hydrological and vegetation response to climate change in a forested
871 mountainous catchment (2016) Modeling Earth Systems and Environment, 2,
872 191 (DOI: 10.1007/s40808-016-0244-1).
873 Berger, T.W., Untersteiner, H., Toplitzer, M. et Neubauer C. (2009) Nutrient fluxes in
874 pure and mixed stands of spruce (Picea abies) and beech (Fagus sylvatica)
875 Plant Soil 322, 317-342.
876 Binkley D. Valentine D., 1991. Fifty-year biogeochemical effects of green ash, white
877 pine, and Norway spruce in a replicated experiment. Forest Ecology and
878 Management 40, 13-25.
879 Blum J.L., Erel Y., (2005). Radiogenic isotopes in weathering and hydrology In
880 Surface and Ground Water, Weathering and Soils (ed. J.I. Drever) 5 Traitise on
881 Geochemistry (eds. H.D. Holland and K.K. Turekian). Elsevier-Pergamon,
882 Oxford. pp.365–392.
883 Blum J.D., Dasch A.A., Hamburg S.P., Yanai R.D., Arthur M.A. (2008) Use of foliar
884 Ca/Sr discrimination and 87Sr/86Sr ratios to determine soil Ca sources to
885 sugar maple foliage in a northern hardwood forest. Biogeochem. 87, 287-296.
886 Bosia C., Chabaux F., Pelt E., France-Lanord C., Morin G., Lavé J., Stille P. (2016) U-Th-
887 Ra variations in the Himalayan River sediments (Gandak river, India):
888 weathering fractionation and/or grain-size sorting? Geochimica et
889 Cosmochimica Acta 193, 176–196.
890 Bosia C., Chabaux F., Pelt E., Cogez A., StilleP., Deloule E., France-Lanord C (2018). U-
891 series disequilibria in minerals from Gandak River sediments (Himalaya),
892 Chemical Geology, 477, 22–34.
893 Bouchez J., von Blanckenburg F., Schuessler J.A. (2013). Modeling novel stable
894 isotope ratios in the weathering zone. Am. J. Sci. 313, 267–308.
895 Bourdon B., Bureau S., Andersen M.B., Pili E., and Hubert E. (2009) Weathering rates
896 from up to bottom in carbonate environment, Chem. Geol. 258, 275-287.
897 Brantley S.L., Goldhaber M.B., and Ragnarsdottir V.K. (2008) Crossing disciplines
898 and scales to understand the Critical Zone, Elements 3, 307-314.
899 Braun J.J., Viers J., Dupré B., Polvé M., Ndam J., and Muller J.P. (1998) Solid/liquid
900 REE fractionation in the lateritic system of Goyoum, East Cameroon: The

implication for the present dynamics of the soil covers of the humid tropical regions. Geochim. Cosmochim. Acta 62, 273-299.

Bullen, T.D., Kendall, C., 1998. Tracing weathering reactions and water flowpaths: a multi- isotope approach. In: Kendall, C., McDonnell, J.J. (Eds.), Isotope Tracers in Catchment Hydrology. Elsevier, Amsterdam, pp. 611–646.

Cenki-Tok B., Chabaux F., Lemarchand D., Schmitt A.-D., Pierret M.-C., Viville D., Bagard M.-L., Stille P., 2009. The impact of water–rock interaction and vegetation on calcium isotope fractionation in soil- and stream waters of a small, forested catchment (the Strengbach case). Geochim. Cosmochim. Acta 73, 2215–2228.

Cerne M., Smodis B., Strok M., Jacimovic R. (2010) Accumulation of ^{226}Ra, ^{238}U and ^{230}Th by wetland plants in a vicinity of U-mill tailings at Zirovski vrh (Slovenia). J Radioanal. Nucl. Chem. 286, 323-327.

Chabaux F., Ben Othman D., J.L. Birck (1994) A new Ra-Ba chromatographic separation and its application for the Ra mass spectrometric maesurement in recent volcanic rocks. Chem. Geol. 114, 191-197. Erratum (1994)Chem. Geol. 116, 301.

Chabaux F., Cohen A.S., O'Nions R.K., Hein J.R. (1995) ^{238}U-^{234}U-^{230}Th chronometry of Fe-Mn crusts: Growth processes and recovery of thorium isotopic ratios of seawater. Geochim. Cosmoch. Acta 59, 633-638.

Chabaux F., O'Nions R.K., Cohen A.S., Hein J.R. (1997). ^{238}U-^{234}U-^{230}Th disequilibrium in hy-drogenous oceanic FeMn crusts: palaeoceanographic record or diagenetic alteration? Geochim. Cosmochim. Acta 61, 3619–3632.

Chabaux F., Hémond C., Allègre C.J. (1999). Timing of magmatic processes in subduction zones: the Lesser Antilles case. Chem. Geol. 153, 171-185

Chabaux F., Riotte J., Schmitt A.-D., Carignan J., Herckès P., Pierret M.-C., Wortham H. (2005) Variations of U and Sr ratios in Alsace and Luxembourg rain waters: origin and hydrogeochemical implications, Comptes Rendus Geoscience 337, 1447-1456.

Chabaux F., Riotte J., and Dequincey O. (2003a) U-Th-Ra fractionation during weathering and river transport. Rev Mineral. Geochem. 52, 533-576.

Chabaux F., Dequincey O., Lévèque J.-J., Leprun J.-C., Clauer N., Riotte J., and Paquet H. (2003b) Tracing and dating recent chemical transfers in wethering profiles by trace element geochemistry and ^{238}U-^{234}U-^{230}Th disequilibria: the exemple of the Kaya lateritic toposequence (Burkina-Faso). C. R. Geoscience 335, 1219-1231.

Chabaux F., Bourdon B., and Riotte J. (2008). U-Series Geochemistry in Weathering Profiles, River Waters and Lakes. Radioactivity in the Environment,13, 49-104.

Chabaux F., Blaes E., Granet M., di Chiara Roupert R., Stille P. (2012) Determination of transfer time for sediments in alluvial plains using ^{238}U-^{234}U-^{230}Th disequilibria: The case of the Ganges river system. CR Geoscience 344, 688-703

Chabaux F., Blaes E., Stille P., di Chiara Roupert R., Pelt E., Dosseto A., Ma L., Buss H., Brantley S.L. (2013). Regolith formation rate from U-series nuclides:

Implications from the study of a spheroidal weathering profile in the Rio Icacos watershed (Puerto Rico) Geochimica et Cosmochimica Acta, 100, 73-95

Chabaux F., Sonke, J.E., Négrel, P., Cloquet C. (2015a,b) Geochemical and isotopic record of anthropogenic activities – Thematic issue dedicated to Jean Carignan (1965–2012). Part 1 : Radiogenic isotopes and elemental geochemistry. Compte Rendus Geoscience, 347, 213-214 - Part 2: Traditional and non-traditional stable isotopes - Compte-Rendus Geoscience, 347, 315-316

Cividini D., Lemarchand D., Chabaux F., Boutin R., Pierret M.-C., 2010. From biological to lithological control of the B geochemical cycle in a forest watershed (Strengbach, Vosges). Geochim. Cosmochim. Acta 74, 3143–3163.

Cremer, M., Prietzel, J. (2017) Soil acidity and exchangeable base cation stocks under pure and mixed stands of European beech, Douglas fir and Norway spruce. Plant Soil 415, 393-405.

DePaolo D., Lee V.E., Christensen J.N., Maher K. (2012) Uranium comminution ages: sediment transport and deposition time scales. C.R. Geosci. 344, 678-687.

DePaolo D., Maher K., Christensen J.N., and McManus J. (2006) Sediment transport time measured with U-series isotopes: Results from ODP North Atlantic drift site 984. Earth Planet. Sci. Lett. 248, 394-410.

Dequincey O., Chabaux F., Clauer N., Sigmarsson O., Liewig N., and Leprun J.-C. (2002) Chemical mobilizations in laterites: Evidence from trace elements and ^{238}U-^{234}U-^{230}Th disequilibria. Geochim. Cosmochim. Acta 66, 1197-1210.

Dequincey O., Chabaux F., Leprun J.-C., H. Paquet, Clauer N., Ph. Larqué (2005) Lanthanide and trace elements mobilisation along a toposequence : clues from Kaya laterite (Burkina Faso) European Journal of Soil Sciences, 57, 816-830

Dewandel, B., Lachassagne, P., Wyns, R., Maréchal, J.C., Krishnamurthy, N.S., 2006. A gen- eralized 3-D geological and hydrogeological conceptual model of granite aquifers controlled by single or multiphase weathering. J. Hydrol. 330, 260–284.

Dosseto, A., Turner, S.P., Chappell, J., 2008. The evolution of weathering profiles through time: new insights from uranium-series isotopes. Earth Planet. Sci. Lett. 274 (3), 359–371.

Dosseto A., Buss H., Chabaux F. (2014) Age and weathering rate of sediments in small-catchments : the role of hillslope erosion. Geochimica et Cosmochimica Acta,132, 238-258.

Dosseto, A., Schaller, M., 2016. The erosion response to Quaternary climate change quantified using uranium isotopes and in situ-produced cosmogenic nuclides. Earth-Sci. Rev. 155, 60–81.

Drouet T., Herbauts J. (2008) Evaluation of the mobility and discrimination of Ca, Sr and Ba in forest ecosystems: consequence on the use of alkaline-earth element ratios as tracers of Ca. Plant Soil 302, 105-124.

Durand S., Chabaux F., Rihs S., Duringer P., Elsass P. (2005) U isotope ratios as tracers of groundwater inputs into surface waters: Example of the Upper Rhine hydrosystem Chemical Geology, 220, 1-19.

Fichter J., Turpault M-P., Dambrine E., and Ranger J. (1998a) Localization of base cations in particle size fractions of acid forest soils _Vosges Mountains, N-E France. Geoderma 82, 295–314.

Fichter J., Turpault M-P., Dambrine E., and Ranger J. (1998b) Mineral evolution of acid forest soils in the Strengbach catchment (Vosges mountains, N-E France). Geoderma 82, 315-340.

Ghaleb, B., Pons-Branchu, E.,Deschamps, P., 2004.Improved method for radium extraction from environmental samples and its analysis by thermal ionization mass spectrometry. J. Anal. At. Spectrom. 7, 906–910.

Gangloff S., Stille P., Pierret M-C., Weber T., and Chabaux F. (2014). Characterization and evolution of dissolved organic matter in acidic forest soil and its impact on the mobility of major and trace elements (case of the Strengbach watershed). Geochim. Cosmochim. Acta 130, 21–41.

Gerzabek M.H., Strebl F., and Temmel B. (1998). Plant uptake of radionuclides in lysimeter experiments. Environ. Pollut. 99, 93-103.

Gontier, A., Rihs, S., Chabaux, F., Lemarchand, D., Pelt, E., Turpault, M.-P. (2015) Lack of bedrock grain size influence on the soil production rate, Geochimica et Cosmochimica Acta, 166, 146-164.

Granet M., Chabaux F., Stille P., Dosseto A., France-Lanord C., Blaes E. (2010) U-series disequilibria in suspended river sediments and implication for sdiment transfer time in alluvial plains : the case of the Himalayan rivers Geochim. Cosmochim. Acta, 74, 2851-2865

Granier A., Bréda N., Biron P.,Villette S. (1999) A lumped water balance model to evaluate duration and intensity of drought constraints in forest stands. Ecol. Model. 116(2–3), 269–283.

Greeman, D.J., Rose, A.W., Washington, J.W., Dobos, R.R., Ciolkosz, E.J., 1999. Geochemistry of radium in soils of the Eastern United States. Appl. Geochem. 14, 365–385.

Hasalová, P., Schulmann K., Tabaud A.-S., Oliot E. (2015) Microstructural evidences for mineralogical inheritance in partially molten rocks: example from the Vosges Mts. Bull. Soc. Géol. France,186, 131-143.

Ignatova N., Dambrine E. (2000) Canopy uptake of N dposition in spruce (Picea abies L. Karst) stands. Annals of Forest Science, Springer Verlag/EDP Sciences, 57, 113-120.

Ivanovich, M. and Harmon, R. S. (eds.) (1992) Uranium-Series Disequilibrium: Application to Earth, Marine, and Environmental Sciences. Clarendon Press, Oxford.

Jeambrun, M., Pourcelot, L., Mercat, C.; Boulet,B., Pelt, E., Chabaux, F., Cagnat X., Gauthier-Lafaye F. (2012) Potential sources affecting the activity concentrations of ^{238}U, ^{235}U, ^{232}Th and some decay products in lettuce and wheat samples. J. Environ. Monit., 14, 2902

Kendal C., Doctor D.H., 2005. Stable isotope applications in hydrologic studies pp. 319– 364. In Surface and Ground Water, Weathering and Soils (ed. J.I. Drever)

5 Traitise on Geochemistry (eds. H.D. Holland and K.K. Turekian). Elsevier-Pergamon, Oxford.
Kronberg B.I., Nesbitt H.W. (1981) Quantification of weathering, soil geochemistry and soil fertility. J. Soil Sci., 32, 453-459.
Ladouche B., Probst A., Viville D., Idir S., Baqué D., Loubet M., Probst J.-L., and Bariac T. (2001) Hydrograph separation using isotopic, chemical and hydrological approaches (Strengbach catchment France). J. Hydrol. 242, 255-274.
Lahd Geagea M., Stille P., Millet M. and Perrone T. (2007) REE characteristics and Pb, Sr and Nd isotopic compositions of steel plant emissions. Sci. Total Environ. 373, 404–419.
Laveuf C. and Cornu S. (2009) A review on the potentiality of Rare Earth Elements to trace pedogenetic processes. Geoderma 154, 1-12.
Lemarchand, D., Cividini, D., Turpault, M.-P. and Chabaux, F. Boron isotopes in different grain size fractions: Exploring past and present water-rock interactions from two soil profiles (Strengbach, Vosges Mountains). *Geochim Cosmochim Ac* **98,** 78–93 (2012).
Lemarchand E., Chabaux F., Vigier N., Millot R., Pierret M-C., 2010. Lithium isotope systematics in a forested granitic catchment (Strengbach, Vosges Mountains, France). Geochim. Cosmochim. Acta 74, 4612-4628.
Li L., Maher K., Navarre-Sitchler A., Druhan J., Meile C., Lawrence C., Moore J., Perdrial J., Sullivan P., Thompson A., Jin L., Bolton E. W., Brantley S. L., Dietrich W.E., Mayer K.U., Steefel C.I., Valocchi A., Zachara J., Kocar B., Mcintosh J., Tutolo B.M., Kumar M., Sonnenthal E., Bao C., Beisman J. (2017) Expanding the role of reactive transport models in critical zone processes. Earth-Science Reviews 165, 280–301.
Lu P., Biron P., Breda N., and Granier A. (1995) Water relations of adult Norway spruce (*Picea abies L.*) under soil drought in the Vosges mountains : water potential, stomatal conductance and transpiration. Ann. Sci. For. 52, 117-129.
Lucas Y., Schmidt A.D., Chabaux F., Clément A., Fritz B., Elsass Ph., Durand S. (2010) Geochemcial tracing and hydrogeochemical modelling of water-rock interactions during salinization of alluvial groundwater (Upper Rhine valley, France) Applied Geochemistry 25, 1644-1663.
Lucas Y., Chabaux F., Schaffhauser T., Fritz B., Ambroise B., Ackerer J., Clément A. (2017) Hydrogeochemical modeling (KIRMAT) of spring and deep borehole water compositions in the small granitic Ringelbach catchment (Vosges Mountains, France). Applied Geochemistry 87, 1–21.
Ma L., Chabaux F., Pelt E., Blaes E., Jin L., Brantley S. (2010) Regolith production rates calculated with uranium-series isotopes at Susquehanna/Shale Hills critical Zone Observatory Earth and Planet Sci. Lett., 297, 211-225
Ma L., Chabaux F., Pelt E., Granet M., Sak P., Gaillardet J., Lebedeva M., Brantley S.B. (2012) The effect of curvature on weathering rind formation: evidence from U-series isotopes in basaltic andesite weathering clasts in Guadeloupe Geochimica et Cosmochimica Acta, 80, 92-107.

Ma L., Chabaux F., West N., Kirby E., Jin L., Brantley S. (2013). Regolith production and transport in the Susquehanna Shale Hills Critical Zone Observatory, Part 1: Insights from U-series isotopes. Journal of Geophysical Research. Earth Surface 118, 722-740

Maher K., DePaolo D.J., Christensen J.N. (2006) U–Sr isotopic speedometer: Fluid flow and chemical weathering rates in aquifers. Geochim. Cosmochim. Acta 70; 4417–4435.

Million J.B., Sartain J.B., Gonzales R.X., Carrier W.D. (1994) Radium-226 and calcium uptake by crops grown in mixtures of sand and clay tailings from phosphate mining. J Environ. Qual. 23, 671-676.

Morgan J.B., Connolly E.L. (2013). Plant-soil interactions: nutrient uptake. Nature Education Knowledge 4 (8), 2.

Négrel Ph., Pauwels H., Chabaux F. (2018) Characterizing Multiple water-rock interactions in the critical zone through Sr-Isotope tracing of surface and groundwater. Applied Geochemistry 93, 102-112.

Opfergelt, S., Delmelle, P., 2012. Silicon isotopes and continental weathering processes: assessing controls on Si transfer to the ocean. CR Geoscience 344, 723–738.

Opfergelt, S., Burton, K.W., Georg, R.B., West, A.J., Guicharnaud, R.A., Sigfusson, B., Siebert, C., Gislason, S.R., Halliday, A.N., 2014. Magnesium retention on the soil exchange complex controlling Mg isotope variations in soils, soil solutions and vegetation involcanic soils, Iceland. Geochim. Cosmochim. Acta 125, 110–130.

Osmond J.K. and Ivanovich M. (1992) Uranium-series mobilization and surface hydrology. In *Uranium series disequilibrium: Application to the earth, marine and environmental Sciences* (Eds. M. Ivanovich and R.S. Harmon), Oxford University Press, New York, pp. 259-288.

Palumbo, B., Bellanca, A., Neri, R., Roe, M.J., 2001.Trace metal partitioning in Fe–Mn nodules from Sicilian soils, Italy. Chem. Geol. 173, 257–269.

Pelt, E., Chabaux, F., Innocent, C., Navarre-Sitchler, A.K., Sak, P.B., Brantley, S.L., 2008. Uranium–thorium chronometry of weathering rinds: rock alteration rate and paleo-isotopic record of weathering fluids. Earth Planet. Sci. Lett. 276, 98–105.

Pelt E., Chabaux F., Stille P., Innocent C., Ghaleb B., Gérard M., Guntzer F., 2013. Atmospheric dust contribution to the budget of U-series nuclides in soils from the Mount Cameroon volcano. Chem. Geol., 341, 147-157

Pierret M.C., Stille P., Prunier J., Viville D., Chabaux F. (2014) Chemical and U-Sr isotopic variations in stream and source wters of the Strengbach watershed (Vosges mountains, France. Hydrol. Earth Syst. 18, 3969-3985.

Pierret M.C., Cotel S., Ackerer P., Beaulieu E., Benarioumlil S., Boucher M., Boutin R., Chabaux F., Dambrine E., Delay F., Fourtet C., Friedmann P., Fritz B., Gangloff S., Girard J.F., Legtchenko A., Viville D., Weill S. and Probst A., 2018. The Strengbach Catchment: a multidisciplinary environmental sentry for 30 years. Vadose Zone Journal 17 (1) DOI: 10.2136/vzj2018.04.0090

1115 Poszwa A., Dambrine E., Pollier B., Atteia O. (2000) A comparison between Ca and Sr
1116 cycling in forest ecosystems. Plant Soil 225, 299–310.
1117 Poszwa, A., Wickman, T., Dambrine, E., Ferry, B., Dupouey, J. L., Helle, G., and Breda,
1118 N. (2003). A retrospective isotopic study of Spruce decline in the Vosges
1119 mountains (France). Water, Air and Soil Pollution: Focus, 3(1), 201-222.
1120 Pourcelot L., Calmon P., Chabaux F., Conil S., Galy C., Granet M., Lascar E., Leclerc E.,
1121 Perrone T., Redon P.-O., Rihs S. (2017) Comparative repartition of ^{226}Ra, ^{238}U,
1122 ^{234}U, ^{230}Th and ^{232}Th in a variety of soils sampled from geological formations in
1123 the NE of the Basin of Paris. Applied Geochemistry, 84, 314-324.
1124 Prunier J., (2008). Etude du fonctionnement d'un écosystème forestier en climat
1125 tempéré, par l'appprot de la géochimie élémentaire et isotopique (Sr, U-Th-
1126 Ra). Cas du bassin versant du Strengbach (Vosges, France). PhD Thesis.
1127 Université Louis Pasteur de Strasbourg, France pp.303.
1128 Prunier J., Chabaux F., Stille P., Gangloff S., Pierret M.C., Viville, D., A. Aubert (2015).
1129 Geochemical and isotopic (Sr,U) monitoring of soil solutions from the
1130 Strengbach catchment (Vosges mountains, France) : Evidence for recent
1131 weathering evolution. Chem. Geol., 417, 289-305
1132 Rihs S., Prunier J., Thien B., Lemarchand D., Pierret M.-C., Chabaux F. (2011) Using
1133 short-lived nuclides of the U- and Th-series to probe the kinetics of colloid
1134 migration in forested soils. Geochim. Cosmochim. Acta 75, 7707-7724.
1135 Rihs S., Gontier A., Pelt E., Fries D., Turpault M-P, Chabaux F. (2016) Behavior of U,
1136 Th and Ra isotopes in soils during a land cover change Chemical Geology 441
1137 106–123.
1138 Riotte J. and Chabaux F. (1999) (^{234}U/^{238}U) Activity ratios in freshwaters as tracers
1139 of hydrological proceses: The Strengbach watershed (Vosges, France).
1140 Geochim. Cosmochim. Acta 63, 1263-1275.
1141 Riotte, F. Chabaux, M. Benedetti, A. Dia, J. Boulègue, M. Gérard, J. Etamé (2003)
1142 234U-238U fractionations in surface waters: the Mount Cameroun case, Chem.
1143 Geol., 202, 365-381.
1144 Schaffhauser T., Chabaux F., Ambroise B., Lucas Y., Stille P., Reuschlé T., Perrone T.,
1145 Fritz B. (2014) Geochemical and isotopic (U, Sr) tracing of water pathways in
1146 the granitic Ringelbach catchment (Vosges Mountains, France) Chemical
1147 Geology, 374-375, 117-127.
1148 Schmitt A.-D., Chabaux F., Stille P. (2003). The calcium riverine and hydrothermal
1149 isotopic fluxes and the oceanic calcium mass balance. Earth Planet. Sci. Lett.
1150 213, 503–518.
1151 Schmitt A.-D., Vigier N., Lemarchand D., Stille P., Millot R., Chabaux F. (2012).
1152 Processes controlling the stable isotope compositions of Li, B, Mg and Ca in
1153 plants, soils and waters: a review. C. R. Geoscience 344, 704–722.
1154 Schmitt A.-D., Cobert F., Bourgeade P., Ertlin D., Labolle F., Gangloff S., Badot P.-M.,
1155 Chabaux F., Stille P. (2013) Calcium isotope fractionation during plant growth
1156 under a limiting nutrient supply, Geochim. Cosmochim. Acta, 100, 73-95.

1157 Schmitt A.D., Gangloff S., Labolle F., Chabaux F., StilleP. (2017). Ca biogeochemical
1158 cycle at the beech tree - soil solution interface from the Strengbach CZO (NE
1159 France): insights from stable Ca and radiogenic Sr isotopes Geochimica et
1160 Cosmochimica Acta 213, 91-109
1161 Schmitt AD, Borrelli N., Ertlen D., Gangloff S., Chabaux F., Osterrieth M. (2018).
1162 Stable calcium isotope speciation and calcium oxalate production within beech
1163 tree (Fagus sylvatica L.) organs. Biogeochemistry, 137,197-217 DOI
1164 10.1007/s10533-017-0411-0
1165 Solovitch-Vella N., Pourcelot L., Chen V.T., Froidevaux P., Gauthier-Lafaye F., Stille P.,
1166 Aubert D. (2007) Comparative migration behaviour of ^{90}Sr, $^{239+240}$Pu and ^{241}Am
1167 in mineral and organic soils of France. Appl. Geochem. 22, 2526-2535.
1168 Soudek P., Podracka E., Vagner M., Vanek T., Petrik P., Tykva R. (2004) ^{226}Ra uptake
1169 from soils into different plant species. J. Radioanal. Nucl. Chem. 282, 187-189.
1170 Steinmann M., Stille P. (1997) Rare earth element behavior and Pb, Sr, Nd isotope
1171 systematics in a heavy metal contaminated soil. Applied Geochemistry, 12,
1172 607-623.
1173 Steinmann M. Stille P. (2009) Controls on transport and fractionation of the rare
1174 earth elements in stream water of a mixed basaltic-granitic catchment basin
1175 (Massif Central, France). Chem. Geol., 254, 1-18.
1176 Stille P., Pourcelot L., Granet M., Pierret M.C., Gueguen F., Perrone T., Morvan G.,
1177 Chabaux F. (2011) Deposition and migration of atmospheric Pb in soils from a
1178 forested silicate catchment today and in the past (Strengbach Case): Evidence
1179 from ^{210}Pb activities and Pb isotope ratios. Chem. Geol., 289, 140-153.
1180 Stille P., Pierret M.-C., Steinmann M., Chabaux F., Boutin R., Aubert D., Pourcelot L.,
1181 Morvan G. (2009) Impact of atmospheric deposition, biogeochemical cycling
1182 and water-mineral interaction on REE fractionation in acidic surface soils and
1183 soil water (the Strengbach case). Chem. Geol. 264, 173-186.
1184 Stille P., Steinmann M., Pierret M.-C., Gauthier-Lafaye F., Chabaux F., Viville D.,
1185 Pourcelot L., Matera V. , Aouad G., Aubert D. (2006) The impact of vegetation
1186 on REE fractionation in stream waters of a small forested catchment (the
1187 Strengbach case). Geochim. Cosmochim. Acta 70, 3217-3230.
1188 Stille P, Schmitt AD, Labolle F, Pierret MC, Gangloff S, Cobert F, Lucot E, Gueguen F,
1189 Brioschi L, Steinmann M, Chabaux F (2012). The suitability of annual tree
1190 growth rings as environmental archives: Evidence from Sr, Nd, Pb and Ca
1191 isotopes in spruce growth rings from the Strengbach watershed CR
1192 Geoscience, 344, 297-311.
1193 Sullivan P. L, Ma L., West J., Jin N. L., Karwan D.L., Noireaux J., Steinhoefel G., Gaines
1194 K.P.,Eissenstat D.M., Gaillardet J., Derry L.A., Meek K., Hynek S.,Brantley S.L. CZ-
1195 tope at Susquehanna Shale Hills CZO: Synthesizing multiple isotope proxies to
1196 elucidate Critical Zone processes across timescales in a temperate forested
1197 landscape. *Chem Geol* 445, 103–119 (2016).
1198 Tabaud A.-S., Janoušek V., Skrzypek E., Schulmann K., Rossi P., Whitechurch H.,
1199 Guerrot C., Paquette J.-L. (2015) Chronology, petrogenesis and heat sources for

successive Carboniferous magmatic events in the Southern–Central Variscan Vosges Mts (NE France). Journal of the Geological Society, 172, 87-102.

Tricca A., Wasserburg G.J., Porcelli D. and Baskaran M. (2001) The transport of U- and Th-series nuclides in a sandy unconfined aquifer. Geochim. Cosmochim. Acta 65, 1187-1210.

Tricca A., Stille P., Steinmann M., Kiefel B., Samuel J., Eikenberg J. (1999) Rare earth elements and Sr and Nd isotopic compositions of dissolved and suspended loads from small river systems in the Vosges mountains (France), the river Rhine and the groundwater. Chem. Geol. 160, 139-158.

Vaniman D.T., Chipera S.J., Bish D.L., Duff M.C., Hunter D.B. (2002). Crystal chemistry of clay-Mn oxide association in soils, fractures and matrix of the Bandelier tuff, Pajarito Mesa, New Mexico. Geochim. Cosmochim. Acta 66, 1349–1374

Viers J., Prokushkin A.S., Pokrovsky O.S., Kirdyanov A.V., Zouiten C., Chmeleff J., Meheut M., Chabaux F., Oliva P., Dupré B. (2015) Zn isotope fractionation in a pristine larch forest on permafrost-dominated soils in Central Siberia. Geochemical Transactions 16, Article number 3

Vigier N., Bourdon B., Turner S., Allègre C.J. (2001). Erosion timescales derived from U-decay series measurements in rivers Earth Planet. Sci. Let. 193, 546–563.

Viville D., Chabaux F., Stille P., Pierret M.-C., Gangloff S., 2012. Erosion and weathering fluxes in granitic basins: The example of the Strengbach catchment (Vosges massif, eastern France). Catena 92, 122–129.

Viville D., Biron P., Granier A., Dambrine E., and Probst A. (1993) Interception in a mountainous declining spruce stand in the Strengbach catchment (Vosges, France). J. Hydrol. 144, 273-282.

Voinot A., Lemarchand D., Collignon C., Granet M., Chabaux F., Turpault MP (2013) Experimental dissolution vs. Transformation of micas in acid soil conditions : clues from boron isotopes Geochimica et Cosmochimica Acta, 117, 144-160.

Wiegand B.A., Chadwick O.A., Vitousek P.M., Wooden J.L. (2005) Ca cycling and isotopic fluxes in forested exosystems in Hawaii. Geophys. Res. Lett. 32, L11404.

Wild B., Daval D., Beaulieu E., Pierret M.P., Viville D., Imfeld G. (2019) In-situ dissolution rates of silicate minerals and associated bacterial communities in the critical zone (Strengbach catchment, France). Geochim. Cosmochim. Acta 249, 95–120.

WRB (2014) World reference base for soil resources 2014. International soil classification system for naming soils and creating legends for soil maps. Update 2015. www.fao.org/ 3/a-i3794e.pdf

Wyns R., Baltassat J.-M., Lachassagne P., Legchenko A., Vairon J., Mathieu F. (2004). Application of proton magnetic resonance soundings to groundwater reserve mapping in weathered basement rocks (Brittany, France). Bull. Soc. Geol. Fr. 175, 21–34.

Table Captions

Table 1 a-c: Major and trace element concentrations, $^{87}Sr/^{86}Sr$ and ($^{238}U/^{234}U$) isotopic ratios, and U-Th-Ra activity ratios in soil grain size fractions (1a); soil solutions, rainwaters and throughfalls (1b); and litter and tree samples (1c).

Table 2a: Mean annual (2004-2006) Ba, U, Th, Ra uptake fluxes by trees for the two experimental plots of the catchment.

Table 2b: Mean annual (2004-2006) Ba, U, Th, Ra fluxes brought by litter deposition and throughfall and circulating in the soil solutions for the two experimental plots of the catchment.

Figure Captions:

Figure 1: Left side: geological map of the Strengbach catchment (from El Gh'Mari, 1995) showing the locations of the spruce (VP) and beech (HP) plots and the precipitation sampling sites (PPT). Right side: schematic presentation of the beech and spruce soil profiles, with the locations of the soil horizons analyzed in this study and the position of the lysimeter plates used to collect the soil solution samples. The surface lysimeter plates allow for sampling soil solutions in zones of high root density (0-30cm) and the deepest lysimeter plates the soil solution below the root zone as in both plots nearly all the fine root biomass resides in the organic layer and upper 0–70 cm of mineral soil. Descriptions of the beech (HP) and spruce (VP) soil profiles can be found in Aubert et al. (2001, 2004), Fichter et al. (1998a, 1998b) and Prunier et al. (2015): the beech soil profile is composed of a ≈ 2 cm thick "O" horizon, a ≈ 20–30 cm thick "A" horizon, which recovers a "B" horizon, whose transition with the saprolite is at ≈ 90–100 cm depth; the spruce soil profile is marked by a ≈2 cm thick "O" horizon, a ≈30–40 cm thick "A" topsoil horizon, and a B horizon, which reaches the granitic saprock at ≈1–1.2 m depth.

Figure 2: Variations in the U concentration as a function of Fe_2O_3 (A), P_2O_5 (B) and variations in the U (C) and Th (D) concentrations as a function of Zr concentrations for the soil size fractions from the spruce and beech soil samples.

Figure 3: Plot of the data in the isochron diagram, ($^{230}Th/^{232}Th$) vs ($^{238}U/^{232}Th$), with the different mixing lines discussed in the text. The Th activity ratios of the primary minerals are calculated by assuming they are at secular equilibrium [($^{230}Th/^{232}Th$) = ($^{238}U/^{232}Th$)].

Figure 4: Variations in the ($^{230}Th/^{232}Th$) and ($^{238}U/^{232}Th$) ratios as a function of Zr concentrations for the soil size fractions from the spruce and beech soil samples.

Figure 5: Variations in the ($^{234}U/^{238}U$) and ($^{230}Th/^{232}Th$) ratios as a function of Zr concentrations for the soil size fractions from the spruce and beech soil samples.

Figure 6: Variation in the ($^{230}Th/^{232}Th$) ratio as a function of P_20_5 concentrations for the soil size fractions from the spruce and beech soil samples.

Figure 7: Variations in the ($^{234}U/^{238}U$) (7a) and ($^{226}Ra/^{230}Th$) (7b) ratios as a function of ($^{230}Th/^{234}U$) ratios for the soil size fractions from the spruce and beech soil samples. Nota Bene: ($^{234}U/^{238}U$) ratios of 3 dusts analyses on the site are given in Prunier et al. (2015). Their U activity ratios range between 0.988 and 1.04, and cannot explain the atypical U activity ratios (i.e. ≈ 0.9) of the deepest soil solutions.

Figure 8a: Plot of the spruce site data in the ($^{226}Ra/^{238}U$) vs ($^{234}U/^{238}U$) diagram. As detailed in the text, the soil solution data collected at 10, 30 and 60 cm and those of the <2 µm and 2-50 µm grain size fractions of the 30-40 cm soil horizon define two linear trends that converge towards the values of the 30 cm soil solutions.

Figure 8b: Plot of the spruce site data in the ($^{226}Ra/^{238}U$) vs Ba/U diagram.

Figure 9: Depth variations in the Sr isotope ratios of the soil solutions from the spruce (VP) and beech (HP) sites. The 0 cm sample points correspond to the throughfall values. The ranges of the vegetation and atmospheric dust values for Sr (data from Guéguen et al., 2012) are also shown. The apatite data are from Aubert et al. (2001). The Sr isotope data for the soil solutions for 1998-1998 are from Aubert et al. (2001), the data from 2004-2006 are from this study; and the data from 2011-2012 are from Schmitt et al. (2017).

Figure 10: ($^{234}U/^{238}U$) vs $^{87}Sr/^{86}Sr$ diagram for the soil solutions, soil grain size fractions, vegetation samples and atmospheric deposits from the beech (HP) and spruce (VP) sites. The albite and apatite Sr data are from Probst et al. (2000) and Aubert et al. (2001), respectively. The curves are the theoretical mixing curves between end-members with U–Sr characteristics similar to those of the 2 µm fractions of the HP beech 30-40 cm soil horizon and the apatite and the albite end-members (see text for details).

Figure 11: Plot of the data in the ($^{230}Th/^{234}U$) vs ($^{226}Ra/^{230}Th$) diagram. The ($^{230}Th/^{234}U$) ratio variations between depths of 10 cm and 70 cm cannot result from the variable contributions of U and Th from litter decay.

Figure 12: Plot of the data in a diagram of the ($^{230}Th/^{232}Th$) ratios against (87Sr/86Sr) isotopic ratios with the different mixing lines discussed in the text.

Figure 13: Plot of the data in the ($^{230}Th/^{232}Th$) vs ($^{234}U/^{238}U$) diagram. The lines in the figure represent possible mixing lines between the different end-members invoked to account for the dispersion of the (HP) beech plot data points in the diagram (see text).

Supplementary Materials

Table EA1a-d: Major and trace element concentrations in the soil solutions from the spruce (1a) and beech (1b) plots, throughfall (1c) and rainwater (1d) for 2003-2006.

Table EA2a: Major (oxide %) and trace element concentrations (mg/kg) in the bedrock (granite), in soil (< 2 mm) and the soil grain size fractions from the

spruce and beech plots.

Table EA2b: Major and trace element concentrations in the litter and different parts of tree samples.

Table EA3a-e: REE concentrations in soil solutions from the spruce plot (a), from the beech plot (b), in throughfalls (c), in the granitic bedrock, in soild (< 2 mm) and tsoil grain size fractions (d) and in vegetation samples (e).

Figure EA1: SEM observations of zircons with evidence of blunted or fractured surfaces (1a), sulfate minerals in VP spruce soils (1b) and soil solutions (1c)

Figure EA2: Variations in some major and trace element concentrations as a function of Fe_20_3 concentrations for the soil size fractions from the spruce and beech soil samples. Fe_20_3 concentrations increase with the decrease in the grain size fraction.

Figure EA3: Plot of soil solution data in binary concentration diagrams (Mn, K vs. Ba; Ba, Ca vs. Mg; Sr, Ba vs. $1/SO_4^{2-}$)

Figure EA4: Chloride, nitrate and sulfate concentrations of the soil solutions from (a) 10 cm and 70 cm depths at the spruce (HP) site and (b) 5 cm, 10 cm, 30 cm and 60 cm depths at the beech (VP) site for 1992–2010.

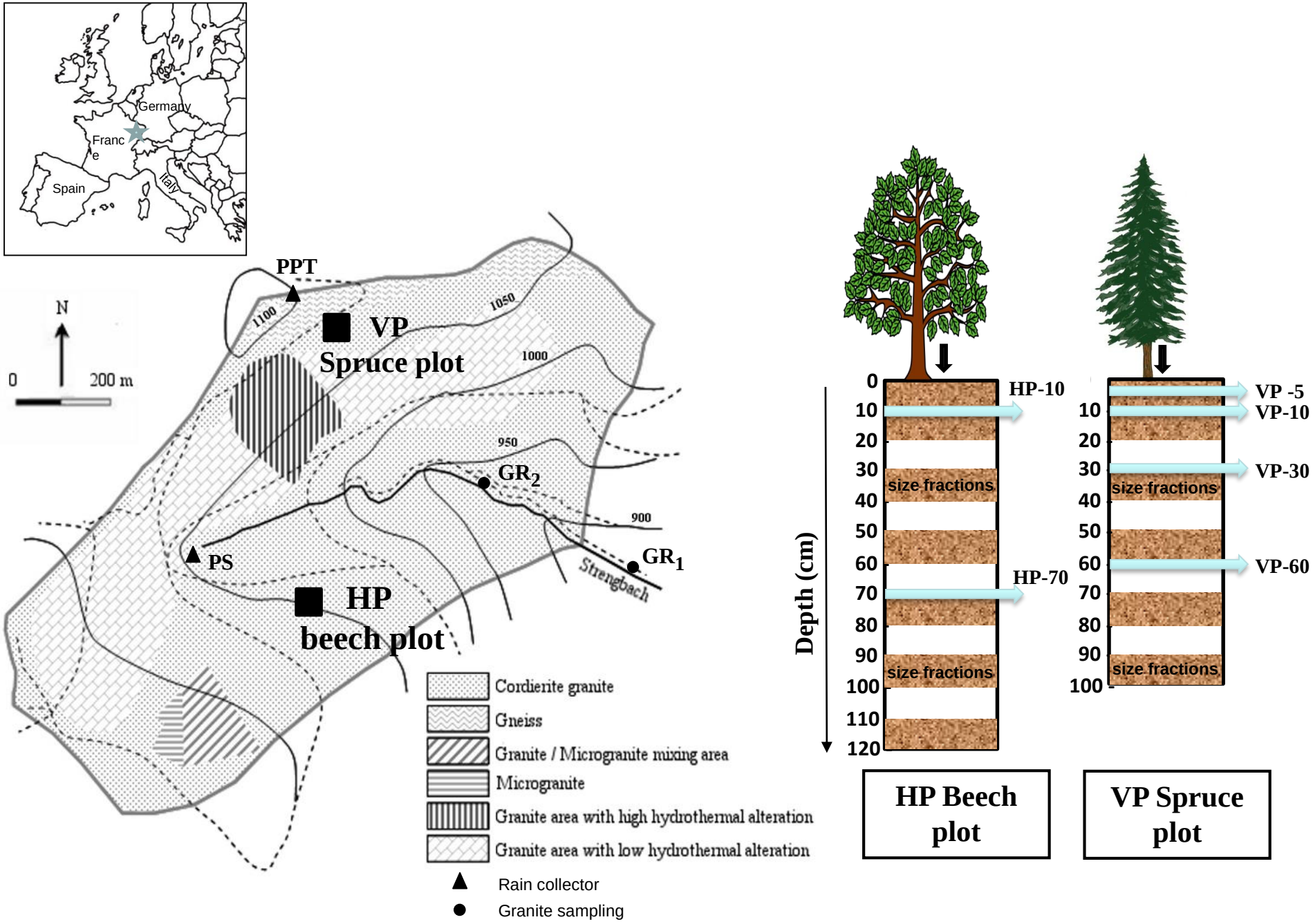
Germany
France
Spain
Italy
PPT
VP
Spruce plot
HP
beech plot
PS
GR2
GR1
Strengbach
1100
1050
1000
950
900
N
0
200 m
Cordierite granite
Gneiss
Granite / Microgranite mixing area
Microgranite
Granite area with high hydrothermal alteration
Granite area with low hydrothermal alteration
Rain collector
Granite sampling
Depth (cm)
0
10
20
30
40
50
60
70
80
90
100
110
120
HP-10
HP-70
size fractions
size fractions
size fractions
VP -5
VP-10
VP-30
VP-60
HP Beech plot
VP Spruce plot

Fig.1

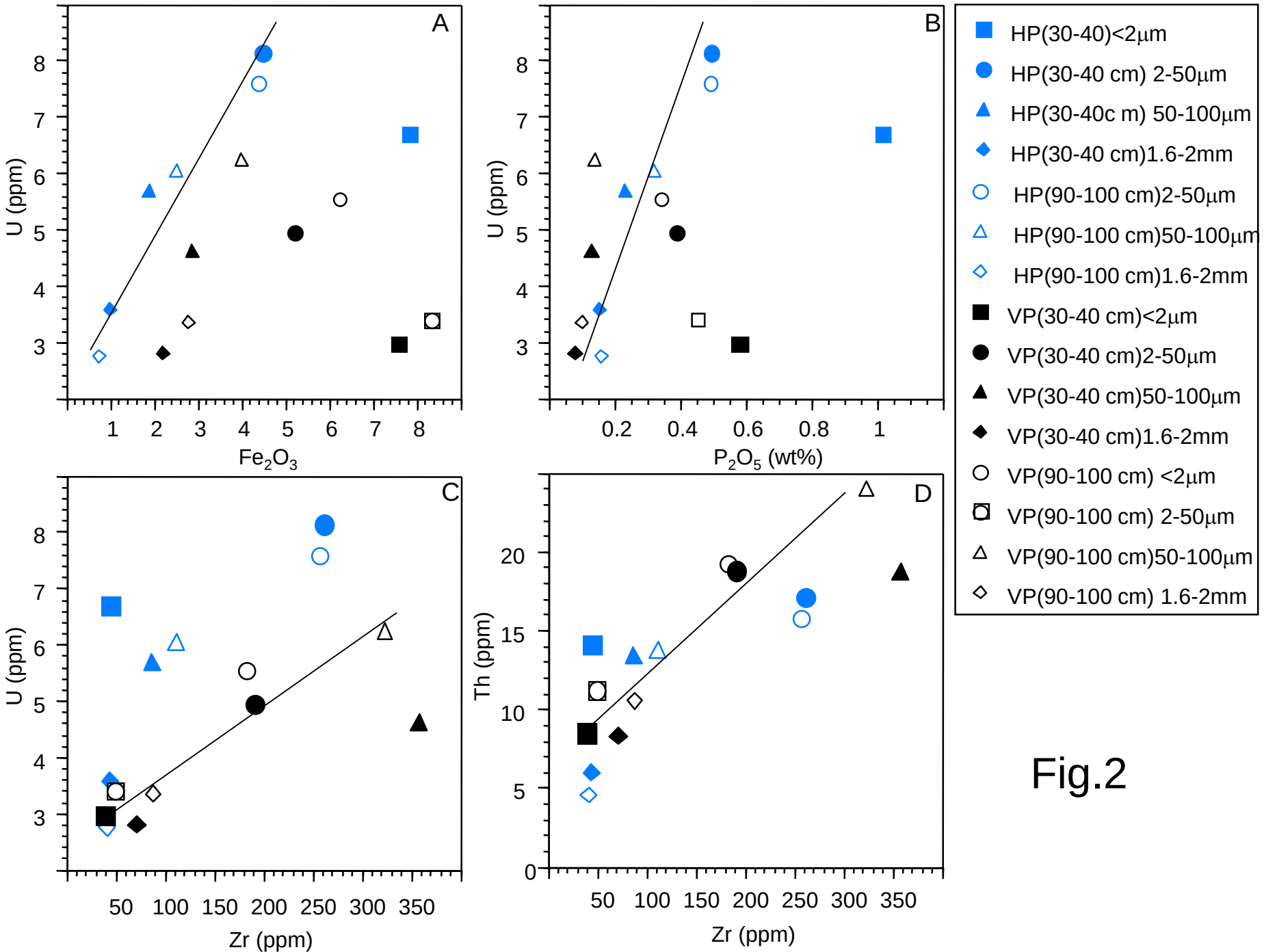
A
B
C
D
U (ppm)
Fe2O3
P2O5 (wt%)
Th (ppm)
Zr (ppm)
HP(30-40)<2µm
HP(30-40 cm) 2-50µm
HP(30-40c m) 50-100µm
HP(30-40 cm)1.6-2mm
HP(90-100 cm)2-50µm
HP(90-100 cm)50-100µm
HP(90-100 cm)1.6-2mm
VP(30-40 cm)<2µm
VP(30-40 cm)2-50µm
VP(30-40 cm)50-100µm
VP(30-40 cm)1.6-2mm
VP(90-100 cm) <2µm
VP(90-100 cm) 2-50µm
VP(90-100 cm)50-100µm
VP(90-100 cm) 1.6-2mm

Fig.2

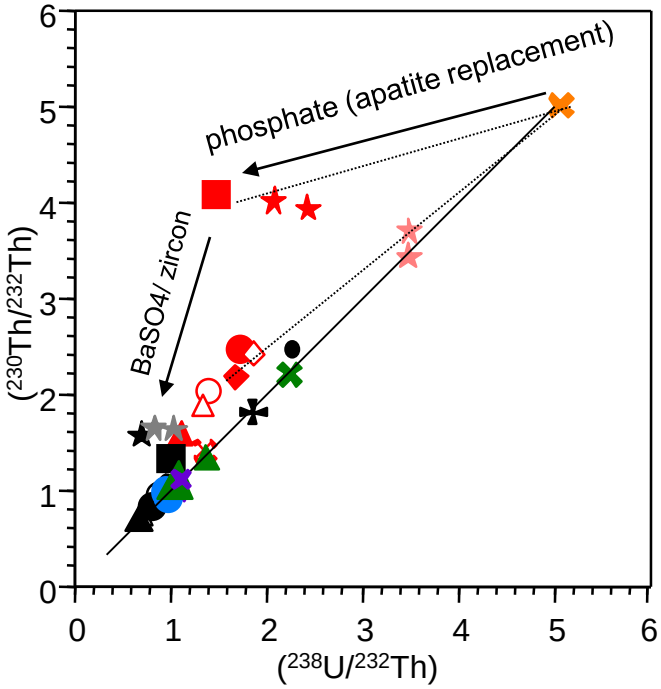

Fig.3

- HP (30-40cm)<2μm
- HP (30-40cm)2-50μm
- HP (30-40cm)50-100μm
- HP (30-40cm)<2mm
- HP (90-100cm)2-50μm
- HP (90-100cm)50-100μm
- HP (90-100cm)1.6-2mm
- VP (30-40cm)<2μm
- VP (30-40cm)2-50μm
- VP (30-40cm) 50-100μm
- VP (30-40cm)1.6-2mm
- VP (90-100cm)<2μm
- VP (90-100cm)2-50μm
- VP (90-100cm)50-100μm
- VP (90-100cm)1.6-2mm
- apatite
- biotite
- albite
- orthoclase
- muscovite
- granite (GR1, GR2)
- soil sol. (HP-10)
- soil sol. (HP-70)
- soil sol. (VP-5)
- soil sol. (VP-10)
- spruce
- beech

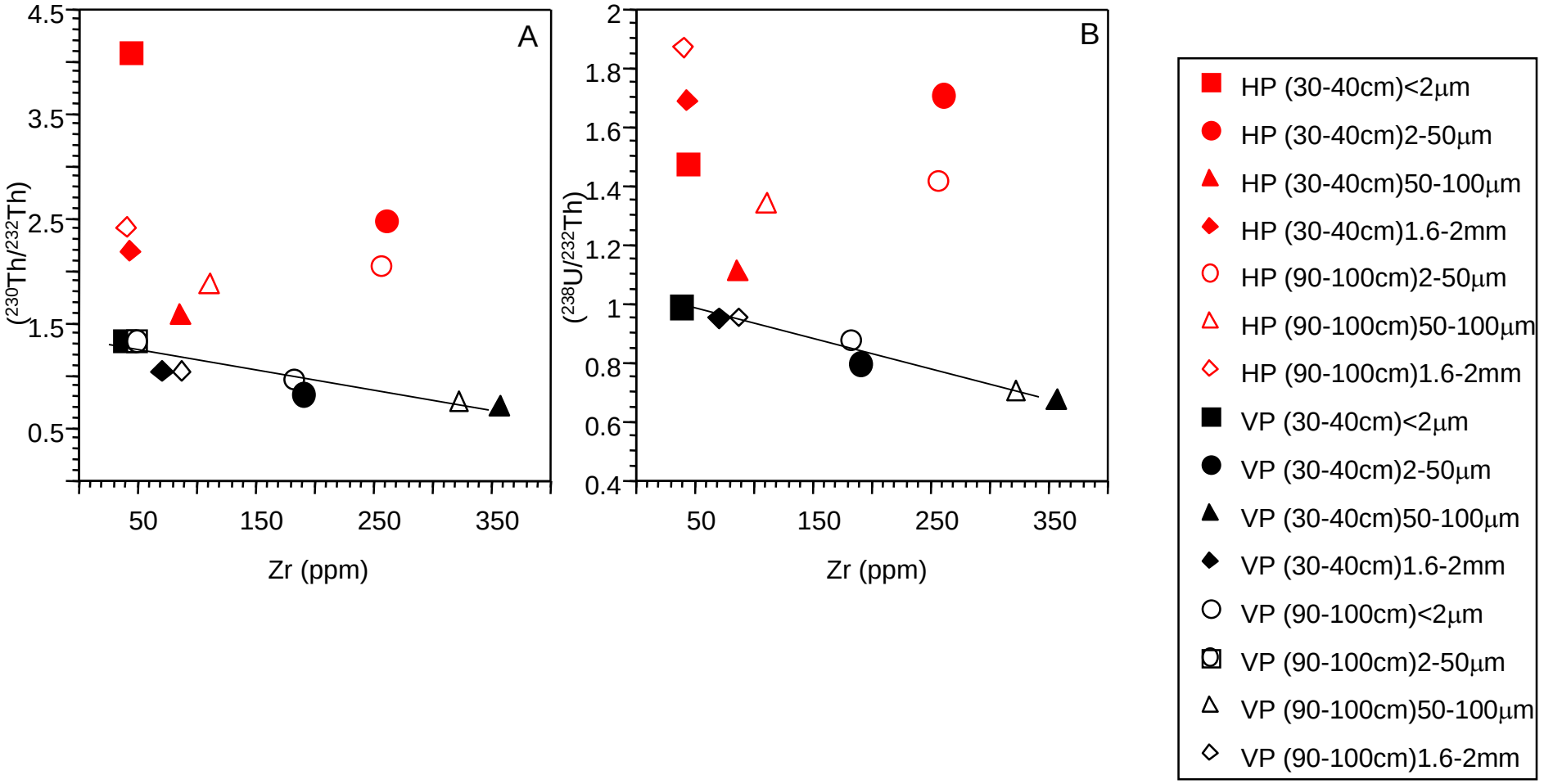
A
B
(230Th/232Th)
(238U/232Th)
Zr (ppm)
Zr (ppm)
4.5
3.5
2.5
1.5
0.5
2
1.8
1.6
1.4
1.2
1
0.8
0.6
0.4
50
150
250
350
HP (30-40cm)<2μm
HP (30-40cm)2-50μm
HP (30-40cm)50-100μm
HP (30-40cm)1.6-2mm
HP (90-100cm)2-50μm
HP (90-100cm)50-100μm
HP (90-100cm)1.6-2mm
VP (30-40cm)<2μm
VP (30-40cm)2-50μm
VP (30-40cm)50-100μm
VP (30-40cm)1.6-2mm
VP (90-100cm)<2μm
VP (90-100cm)2-50μm
VP (90-100cm)50-100μm
VP (90-100cm)1.6-2mm

Fig.4

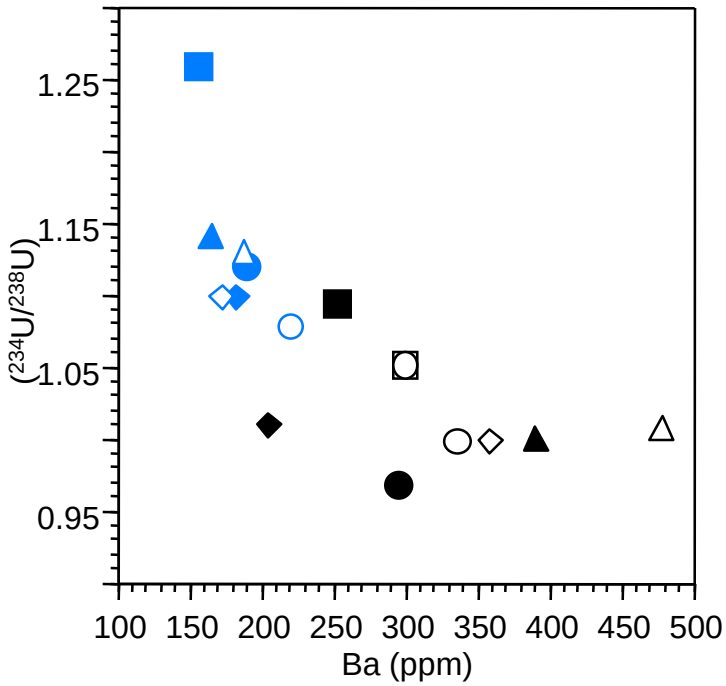
1.25
1.15
1.05
0.95
(234U/238U)
100 150 200 250 300 350 400 450 500
Ba (ppm)

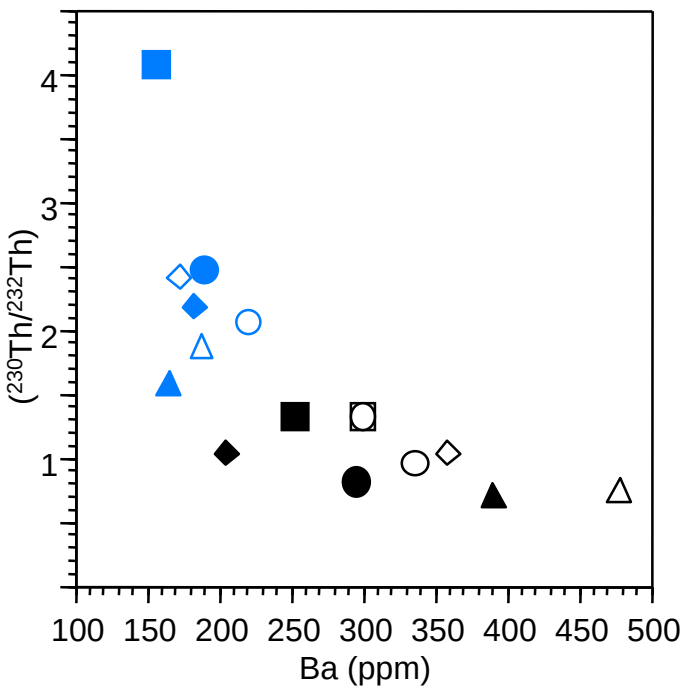
4
3
2
1
(230Th/232Th)
100 150 200 250 300 350 400 450 500
Ba (ppm)

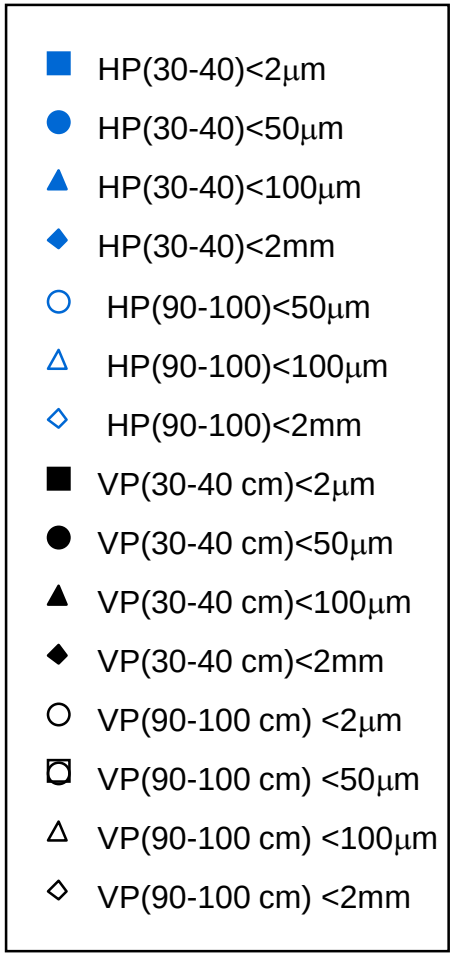
HP(30-40)<2μm
HP(30-40)<50μm
HP(30-40)<100μm
HP(30-40)<2mm
HP(90-100)<50μm
HP(90-100)<100μm
HP(90-100)<2mm
VP(30-40 cm)<2μm
VP(30-40 cm)<50μm
VP(30-40 cm)<100μm
VP(30-40 cm)<2mm
VP(90-100 cm) <2μm
VP(90-100 cm) <50μm
VP(90-100 cm) <100μm
VP(90-100 cm) <2mm

Fig.5

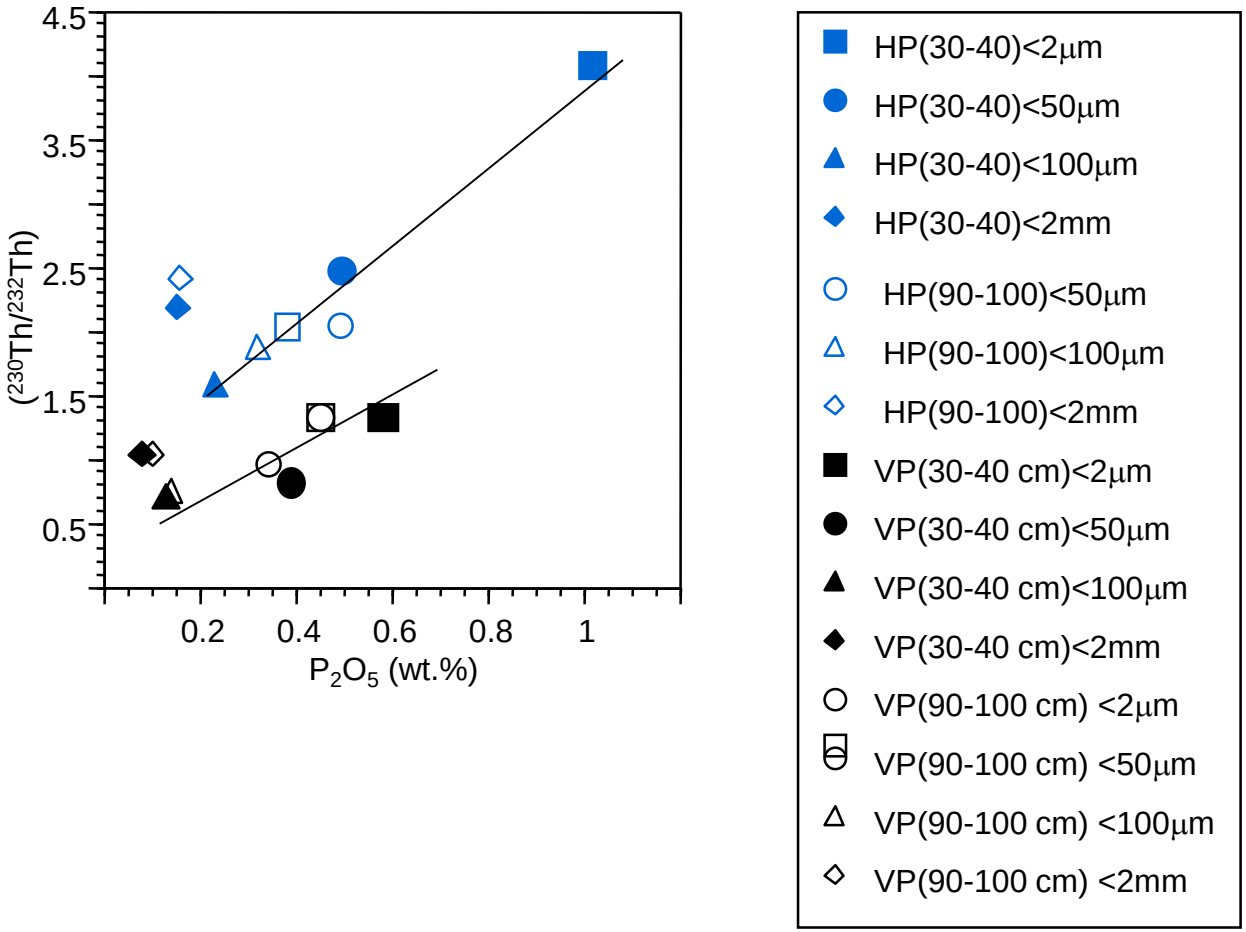
4.5
3.5
2.5
1.5
0.5
0.2
0.4
0.6
0.8
1
(230Th/232Th)
P2O5 (wt.%)
HP(30-40)<2μm
HP(30-40)<50μm
HP(30-40)<100μm
HP(30-40)<2mm
HP(90-100)<50μm
HP(90-100)<100μm
HP(90-100)<2mm
VP(30-40 cm)<2μm
VP(30-40 cm)<50μm
VP(30-40 cm)<100μm
VP(30-40 cm)<2mm
VP(90-100 cm) <2μm
VP(90-100 cm) <50μm
VP(90-100 cm) <100μm
VP(90-100 cm) <2mm

Fig.6

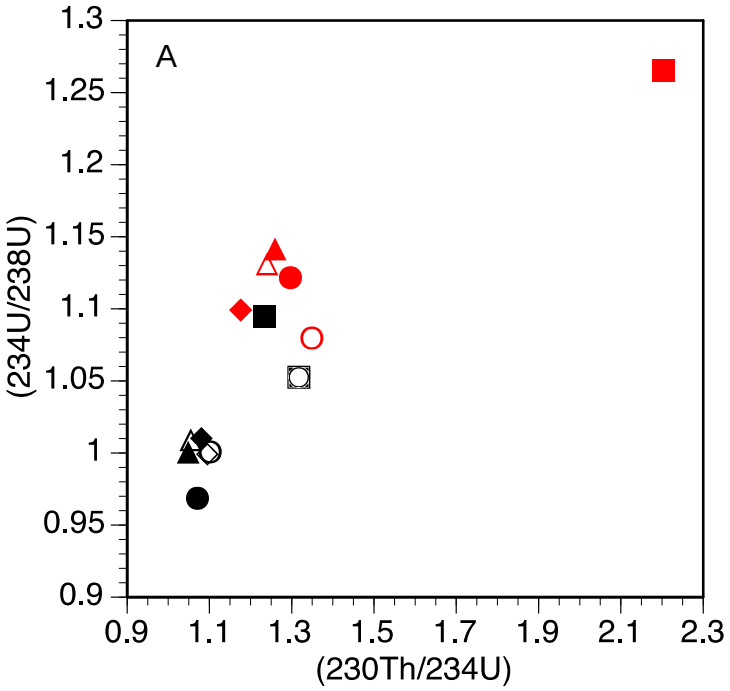
A
(234U/238U)
(230Th/234U)
1.3
1.25
1.2
1.15
1.1
1.05
1
0.95
0.9
0.9
1.1
1.3
1.5
1.7
1.9
2.1
2.3

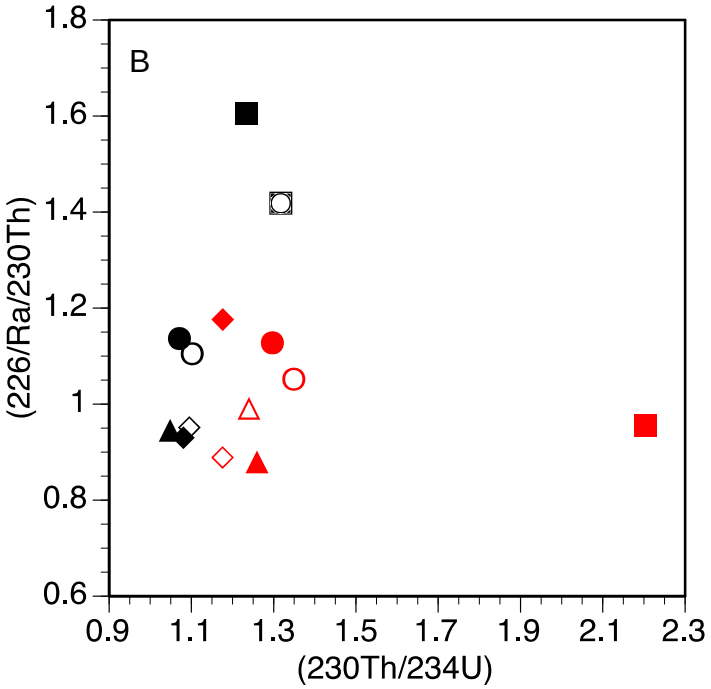
B
(226/Ra/230Th)
(230Th/234U)
1.8
1.6
1.4
1.2
1
0.8
0.6
0.9
1.1
1.3
1.5
1.7
1.9
2.1
2.3

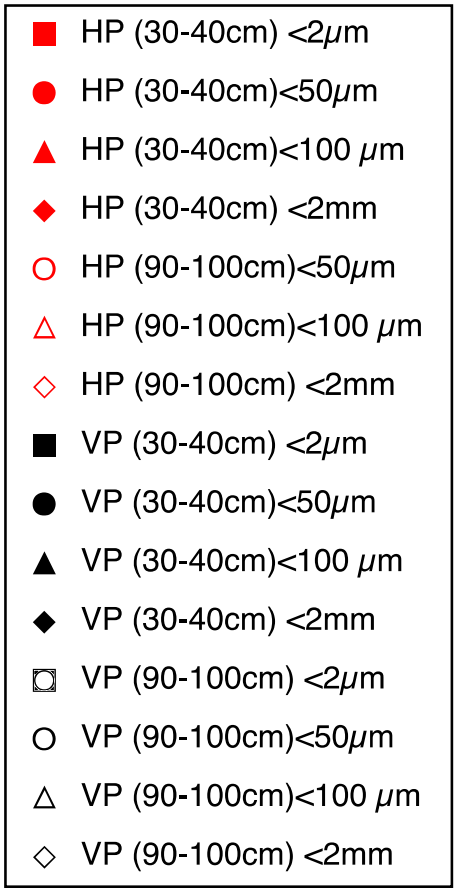
HP (30-40cm) <2μm
HP (30-40cm)<50μm
HP (30-40cm)<100 μm
HP (30-40cm) <2mm
HP (90-100cm)<50μm
HP (90-100cm)<100 μm
HP (90-100cm) <2mm
VP (30-40cm) <2μm
VP (30-40cm)<50μm
VP (30-40cm)<100 μm
VP (30-40cm) <2mm
VP (90-100cm) <2μm
VP (90-100cm)<50μm
VP (90-100cm)<100 μm
VP (90-100cm) <2mm

Fig.7

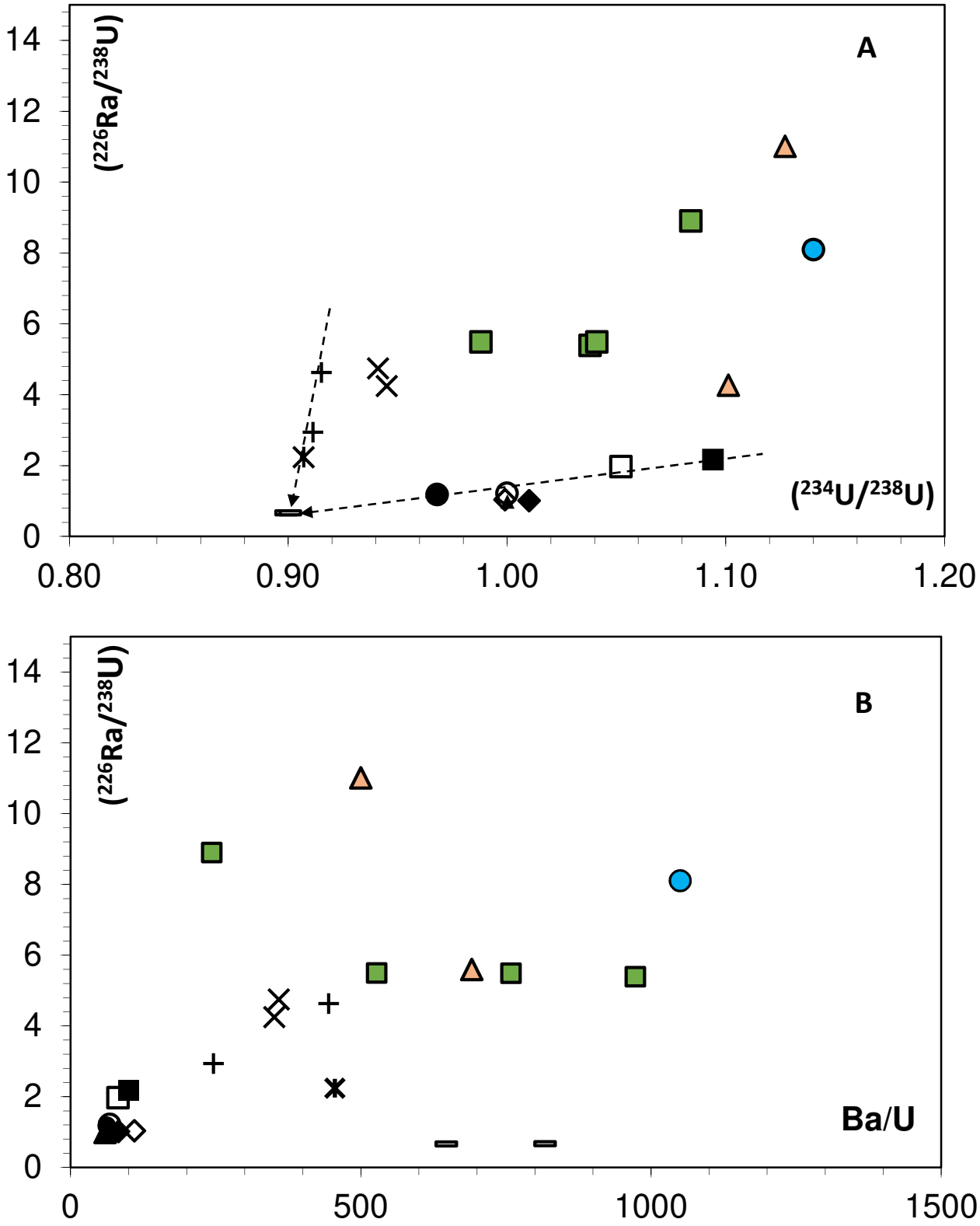
A
(226Ra/238U)
(234U/238U)
0
2
4
6
8
10
12
14
0.80
0.90
1.00
1.10
1.20
B
(226Ra/238U)
Ba/U
0
2
4
6
8
10
12
14
0
500
1000
1500
Rain water
throughfalls
<2 µm (VP 30-40)
2-50 µm (VP 30-40)
50-100 µm (VP 30-40)
1.6 - 2 mm (VP 30-40)
<2 µm (VP 90-100)
50-100µm (VP 90-100)
1.6 - 2 mm (VP 90-100)
vegetation
Soil sol. -5cm
soil sol. -10cm
soil sol. -30cm
soil sol. -60cm

Figure 8

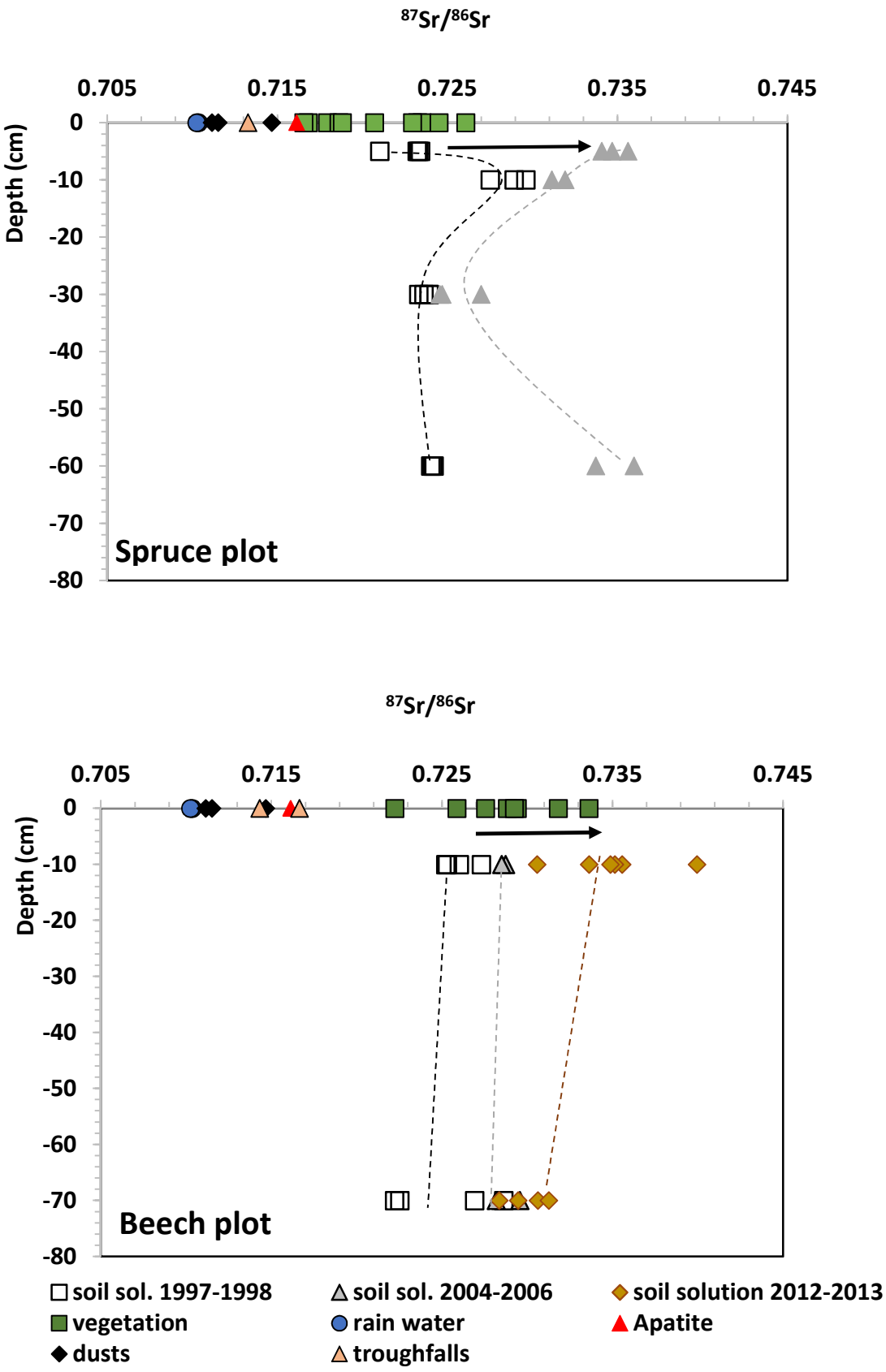
87Sr/86Sr
0.705
0.715
0.725
0.735
0.745
Depth (cm)
0
-10
-20
-30
-40
-50
-60
-70
-80
Spruce plot
87Sr/86Sr
0.705
0.715
0.725
0.735
0.745
Depth (cm)
0
-10
-20
-30
-40
-50
-60
-70
-80
Beech plot
soil sol. 1997-1998
soil sol. 2004-2006
soil solution 2012-2013
vegetation
rain water
Apatite
dusts
troughfalls

Figure 9

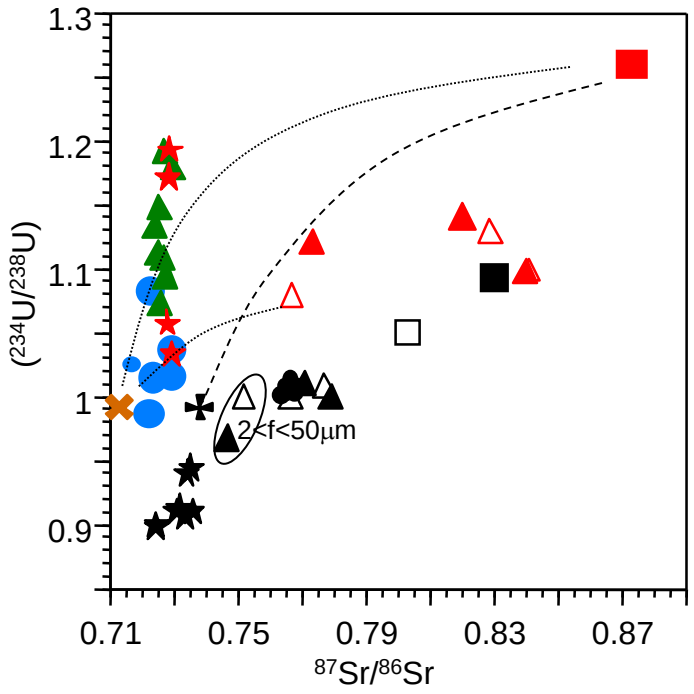

- VP (30-40cm) <2µm
- VP (30-40cm) (2µm<-<2mm)
- VP (90-100cm) <2µm
- VP (90-100cm) (2µm<-<2mm)
- HP (30-40cm) <2µm
- HP (30-40cm) (2µm<-<2mm)
- HP (90-100cm) (2µm<-<2mm)
- soil sol. VP
- soil sol. HP
- spruce
- litter spruce
- beech
- litter beech
- apatite
- albite

Fig.10

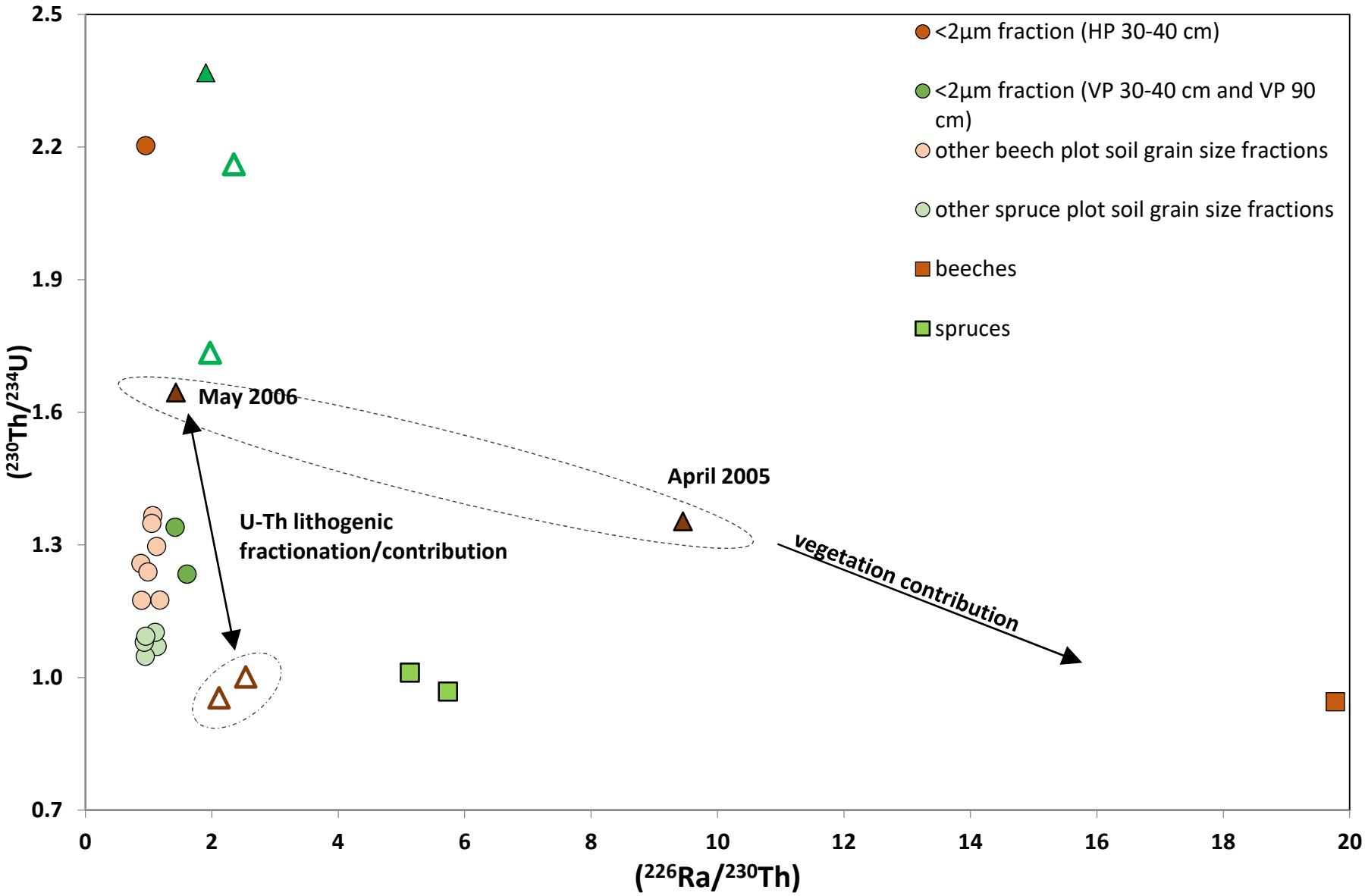
2.5
2.2
1.9
1.6
1.3
1.0
0.7
0
2
4
6
8
10
12
14
16
18
20
(230Th/234U)
(226Ra/230Th)
<2µm fraction (HP 30-40 cm)
<2µm fraction (VP 30-40 cm and VP 90 cm)
other beech plot soil grain size fractions
other spruce plot soil grain size fractions
beeches
spruces
May 2006
April 2005
U-Th lithogenic fractionation/contribution
vegetation contribution

Figure 11

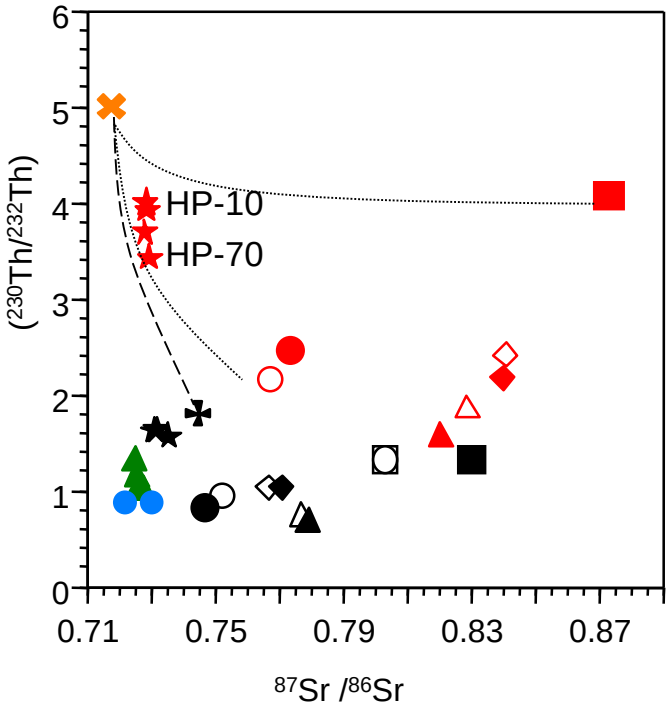

Fig.12

HP (30-40cm)<2μm
HP (30-40cm)<50μm
HP (30-40cm)<100μm
HP (30-40cm)<2mm
HP (90-100cm)<50μm
HP (90-100cm)<100μm
HP (90-100cm)<2mm
VP (30-40cm)<2μm
VP (30-40cm)<50μm
VP (30-40cm)<100μm
VP (30-40cm)<2μm
VP (90-100cm)<2μm
VP (90-100cm)<50μm
VP (90-100cm)<100μm
VP (90-100cm)<2mm
apatite
plagioclase
soil sol. HP
soil sol. VP
spruce
beech

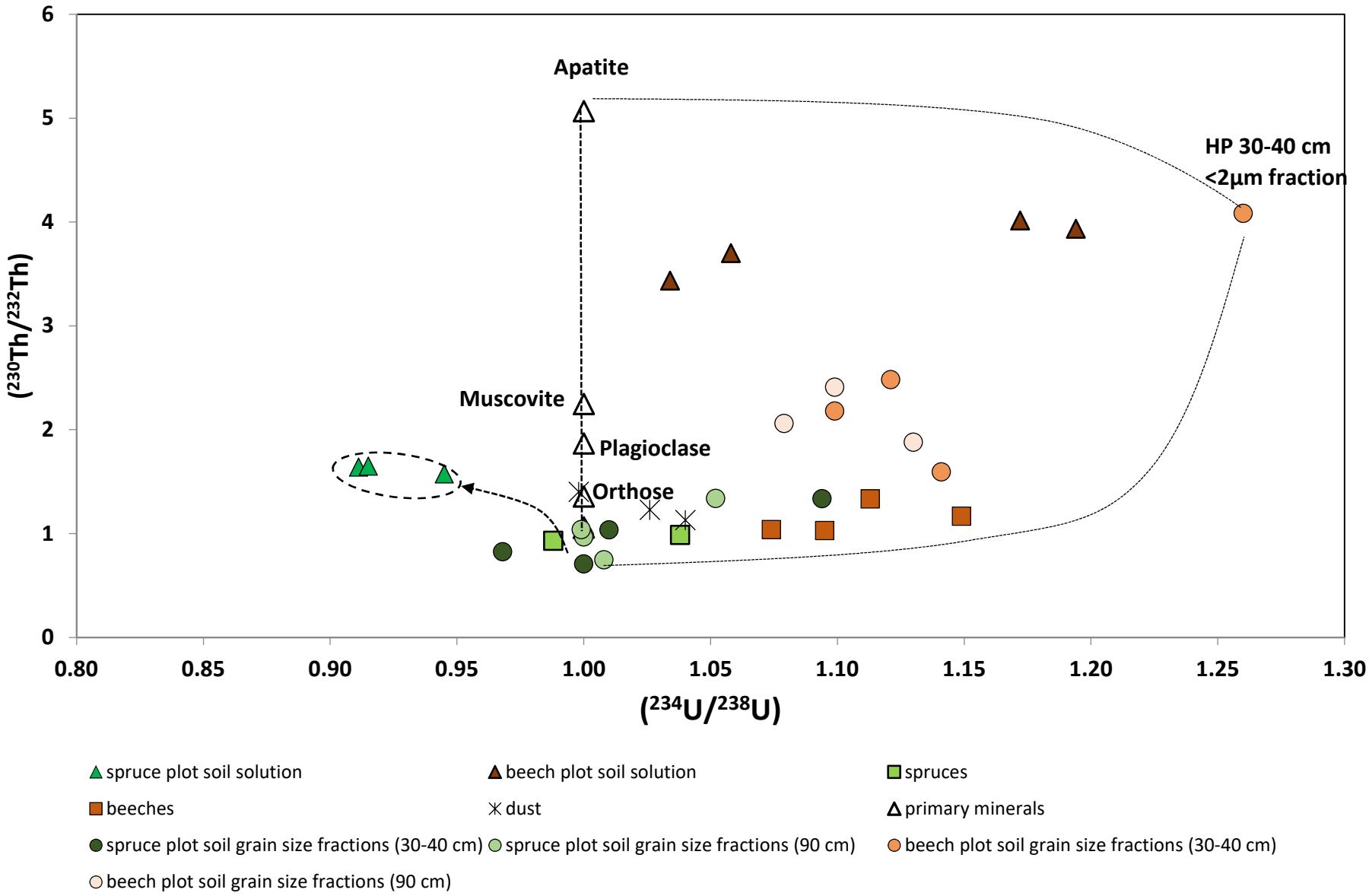
Apatite
HP 30-40 cm
<2µm fraction
Muscovite
Plagioclase
Orthose
(230Th/232Th)
(234U/238U)
0
1
2
3
4
5
6
0.80
0.85
0.90
0.95
1.00
1.05
1.10
1.15
1.20
1.25
1.30
spruce plot soil solution
beech plot soil solution
spruces
beeches
dust
primary minerals
spruce plot soil grain size fractions (30-40 cm)
spruce plot soil grain size fractions (90 cm)
beech plot soil grain size fractions (30-40 cm)
beech plot soil grain size fractions (90 cm)

Figure 13

Table 1 a : Major and trace element concentrations, $^{87}Sr/^{86}Sr$ and U-Th-Ra activity ratios in soil grain size fractions of two horizons 30-40 cm and 90-100 cm from spruce (VP) and beech (HP) profiles.

Site	Depth (cm)	Sample name	Size of the soil grain fractions	Fe_2O_3 wt %	MnO_2 wt %	P_2O_5 wt %	Ba mg/kg	Zr mg/kg	Pb mg/kg	Sr mg/kg	U mg/kg	Th mg/kg	Ra pg/kg	$^{87}Sr/^{86}Sr$ (2σ)	$^{234}U/^{238}U$ (2σ)	$(^{230}Th/^{232}Th)$ (2σ)	$(^{238}U/^{232}Th)$ (2σ)	$(^{226}Ra/^{238}U)$ (2σ)	$(^{226}Ra/^{230}Th)$ (2σ)
VP spruce site	30-40	VP-F1A	<2 µm	5.89	0.115	0.580	251	39.0	99.6	36.5	2.508	7.635	1820	0.83003 ± 2	1.094 ± 3	1.34 ± 1	0.99 ± 1	2.17 ± 3	1.60 ± 2
		VP-F2A	2-50 µm	4.04	0.086	0.390	295	190	85.3	133	4.717	17.83	1858	0.74672 ± 2	0.968 ± 3	0.826 ± 8	0.797 ± 8	1.18 ± 2	1.14 ± 2
		VP-F3A	50-100 µm	2.22	0.032	0.130	390	358	49.3	66.1	6.587	29.31	2183	0.77931± 1	1.000 ± 3	0.710 ± 7	0.677 ± 7	0.99 ± 2	0.94 ± 1
		VP-F4A	1.6-2 mm	1.71	0.049	0.080	205	71.0	53.9	47.1	2.488	7.884	844.9	0.77082 ± 1	1.010 ± 3	1.04 ± 1	0.95 ± 1	1.01 ± 2	0.93 ± 1
	90-100	VP-F1B	< 2µm	6.47	0.156	0.450	299	49.0	40.7	36.9	3.653	11.37	2402	0.80289 ± 1	1.052 ± 3	1.34 ± 1	0.97 ± 1	1.96 ± 3	1.42 ± 2
		VP-F2B	2-50 µm	4.85	0.155	0.340	335	183	51.0	102	4.965	17.01	2022	0.75209 ± 1	1.000 ± 3	0.97 ± 1	0.879 ± 9	1.22 ± 2	1.10 ± 2
		VP-F3B	50-100 µm	3.10	0.112	0.140	478	323	132	72.3	5.464	23.33	n.d	0.77721 ± 1	1.008 ± 3	0.750 ± 8	0.706 ± 7	n.d	n.d
		VP-F4B	1.6-2 mm	2.16	0.188	0.100	359	88.0	50.6	55.8	3.271	10.35	1139	0.76657 ± 8	0.999 ± 3	1.04 ± 1	0.95 ± 1	1.04 ± 2	0.95 ± 1
HP beech site	30-40	HP-F1A	< 2µm	6.09	0.076	1.02	155	44.2	38.0	20.9	6.404	13.12 (12.09)	5674	0.87288 ± 2 (0.87289±2)	1.260 ± 3 (1.265±3)	4.09 ± 4 (4.10 ± 4)	1.47 ± 2	2.65 ± 4	0.95 ± 1
		HP-F2A	2-50 µm	3.48	0.042	0.494	188	260.6	22.9	57.3	7.425	13.10	4071	0.77335 ± 2	1.121 ± 3	2.48 ± 3	1.71 ± 2	1.64 ± 3	1.13 ± 2
		HP-F3A	50-100 µm	1.46	0.018	0.231	165	86.6	20.8	45.7	5.286	14.34	2234	0.82036 ± 2	1.141 ± 3	1.60 ± 2	1.11 ± 1	1.26 ± 2	0.88 ± 1
		HP-F4A	1.6-2 mm	0.77	0.032	0.154	183	43.9	20.4	31.7	3.253	5.803	1424	0.8402 ± 2	1.099 ± 3	2.18 ± 2	1.69 ± 2	1.31 ± 2	1.18 ± 2
	90-100	HP-F2B	2-50 µm	3.40	0.038	0.490	219	256	41.9	71.6	7.425	15.79	3799	0.76688 ± 1	1.079 ± 3	2.06 ± 2	1.42 ± 2	1.53 ± 2	1.05 ± 2
		HP-F3B	50-100 µm	1.94	0.036	0.320	188	111	70.5	49.8	5.809	13.02	2692	0.82885 ± 1 (0.82882±4)	1.130 ± 3	1.88 ± 2	1.34 ± 1	1.38 ± 2	0.99 ± 2
		HP-F4B	1.6-2 mm	0.57	0.013	0.160	172	41.0	42.3	34.7	3.401	5.487	1307	0.84092 ± 2	1.099 ± 3	2.41 ± 2	1.87 ± 2	1.15 ± 2	0.89 ± 1

U-Th-Ra data were determined by isotope dilution (n.d.: no defined). Replicates in brackets.

Table 1b: Major and trace element concentrations, $^{87}Sr/^{86}Sr$ and U-Th-Ra activity ratios in soil solutions, rainwaters and throughfalls from the Strengbach catchment.

Site	Sample name	Depth (cm)	date	SO_4^{2-} mmol/L	DOC mg/kg	Fe mg/kg	Ba µg/kg	Sr µg/kg	U µg/kg	Th µg/kg	Ra fg/kg	$^{87}Sr/^{86}Sr$ (2σ)	$(^{234}U/^{238}U)$ (2σ)	$(^{230}Th/^{232}Th)$ (2σ)	$(^{238}U/^{232}Th)$ (2σ)	$(^{226}Ra/^{238}U)$ (2σ)	$(^{226}Ra/^{230}Th)$ (2σ)
VP spruce site (7°1983 E, 48°216N)	VP-5 (soil solution)	-5	29/03/2005	0.040	16.7	0.470	14.3	4.18	0.0400	0.0740	63.38	0.73407 ± 2	0.941 ± 3	n.d	n.d	4.75 ± 7	n.d
		-5	22/05/2006	0.030	26.6	0.690	13.9	4.24	0.0379	0.1620	54.00	0.73561 ± 2	0.945 ± 4	1.58 ± 2	0.704 ± 7	4.25 ± 6	1.90 ± 3
	VP-10 (soil solution)	-10	29/03/2005	0.038	10.9	0.270	10.9	2.33	0.0444	0.1230	44.14	0.73114 ± 5	0.9112 ± 8	1.64 ± 2	1.04 ± 1	2.94 ± 4	1.97 ± 3
		-10	22/05/2006	0.030	13.7	0.290	14.3	3.17	0.0321	0.1160	49.80	0.73191 ± 2	0.915 ± 4	1.65 ± 2	0.838 ± 8	4.63 ± 7	2.35 ± 4
	VP-30 (soil solution)	-30	29/03/2005	0.045	4.38	0.026	30.3	3.09	0.0370	0.0350	8.300	0.72468 ± 2	0.899 ± 3	n.d	n.d	0.670 ± 1	n.d
		-30	22/05/2006	0.037	4.97	0.024	19.3	2.11	0.0298	0.0440	6.700	0.72455 ± 2	0.901 ± 1	n.d	n.d	0.667 ± 1	n.d
	VP-60 (soil solution)	-60	02/11/2004	0.049	2.61	0.003	17.8	2.65	0.0120	0.0070	n.d	0.73597 ± 2	0.911 ± 4	n.d	n.d	n.d	n.d
		-60	29/03/2005	0.052	1.76	0.008	13.7	3.22	0.0300	0.0050	22.64	0.73372 ± 2	0.907 ± 4	n.d	n.d	2.24 ± 3	n.d
HP beech site (7°1963 E, 48°211 N)	HP-10 (soil solution)	-10	29/03/2005	0.031	5.74	0.200	4.38	1.44	0.0380	0.0470	194.5	0.72872 ± 2	1.194 ± 3	3.94 ± 4	2.44 ± 2	15.1 ± 2	9.4 ± 1
		-10	22/05/2006	0.012	12.93	0.470	3.03	1.05	0.0740	0.1080	68.70	0.72850 ± 2	1.172 ± 2	4.02 ± 4	2.08 ± 2	2.76 ± 4	1.43 ± 2
	HP-70 (soil solution)	-70	29/03/2005	0.027	2.26	0.009	4.52	0.68	0.0290	0.0253	26.08	0.72817 ± 2	1.058 ± 3	3.70 ± 4	3.50 ± 4	2.68 ± 4	2.53 ± 4
		-70	22/05/2006	0.038	2.78	0.010	5.03	1.05	0.0310	0.0260	21.30	0.72956 ± 2	1.034 ± 4	3.44 ± 3	3.49 ± 4	2.09 ± 3	2.11 ± 3
Top of watershed	PPT (rain water)		31/05/2005	0.018	0.81	0.003	0.63	0.90	0.0006	n.d	1.100	0.71024 ± 4	1.140 ± 3	n.d	n.d	5.25 ± 8	n.d
	PS (rain water)		03/05/2005	0.013	0.72	0.007	3.19	0.81	0.0006	n.d	1.600	n.d	n.d	n.d	n.d	8.1 ± 1	n.d
VP spruce site (7°1983 E, 48°216N)	VP-PL5 (Throughfall)		29/03/2005	0.202	19.0	0.050	27.8	16.0	0.0028	*0.006*	27.97	n.d	n.d	n.d	n.d	21.9 ± 3	n.d
			31/05/2005	0.025	4.1	0.030	11.0	2.77	0.0029	*0.001*	4.100	0.71327 ± 2	1.101 ± 3	n.d	n.d	4.27 ± 6	n.d
HP beech site (7°1963 E, 48°211 N)	HP-PLH (Throughfall)		29/03/2005	0.041	4.47	0.010	4.14	5.26	0.0060	*0.007*	11.32	n.d	n.d	n.d	n.d	6.00 ± 8	n.d
			31/05/2005	0.033	9.04	0.010	0.510	0.56	0.0010	*0.005*	3.800	0.71664 ± 3	1.127 ± 4	n.d	n.d	11.0 ± 2	n.d

U-Th-Ra italic data were determined by ICP-MS and the others by isotope dilution (n.d.: no defined). Replicates in brackets.

Table 1c : Major and trace element concentrations, $^{87}Sr/^{86}Sr$ and U-Th-Ra activity ratios in litter and in different parts of tree samples.

Site	Sample	Sample name	Date	Ca mg/kg	K mg/kg	Mn mg/kg	Ba mg/kg	Sr mg/kg	U µg/kg	Th µg/kg	Ra pg/kg	$^{87}Sr/^{86}Sr$ (2σ)	$(^{234}U/^{238}U)$ (2σ)	$(^{230}Th/^{232}Th)$ (2σ)	$(^{238}U/^{232}Th)$ (2σ)	$(^{226}Ra/^{238}U)$ (2σ)	$(^{226}Ra/^{230}Th)$ (2σ)
VP spruce site	Litter	VP-LT	21/06/2004	3487	992.5	1038	13.8	7.17	*19.6*	*59.0*	n.d	0.71653 ± 2	1.026 ± 5	n.d	n.d	n.d	n.d
	Sapwood	VP-SW	23/05/2006	594	338.8	1117	28.4	6.25	0.3830	1.154	10.13	0.72915 ± 4	1.017 ± 4	n.d	n.d	79 ± 1	n.d
	Tree roots (Ø = 2-5 mm)	VP-MR	23/05/2006	2647	3415	81.1	29.55	5.89	56.01	173.3	102.9	0.72195 ± 3	0.988 ± 3	0.932 ± 9	0.97 ± 1	5.49 ± 8	5.73 ± 9
	Top tree branches (Ø = 2-5 mm)	VP-TB	15/05/2007	2148	5140	91.6	9.32	5.25	9.583	30.67	17.29	0.71934 ± 3	1.038 ± 3	0.99 ± 1	0.941 ± 9	5.39 ± 8	5.13 ± 8
	Needles (> 1yr)	VP-ON4	15/05/2007	1736	4080	88.6	1.42	1.20	1.876	*5.92*	0.7057	0.72345 ± 3	1.016 ± 3	n.d	n.d	1.12 ± 2	n.d
	Needles (< 1yr)	VP-YN1	15/05/2007	458	11293	141	0.601	0.36	2.467	*5.91*	7.349	0.72222 ± 2	1.084 ± 3	n.d	n.d	8.9 ± 1	n.d
HP beech site	Litter	HP-LT	21/06/2004	5766	2043	757	16.3	12.7	*15.5*	*35.2*	n.d	n.d	1.049 ± 4	n.d	n.d	n.d	n.d
	Sapwood	HP-SW	21/09/2005	182	273.2	16.2	7.41	2.69	0.234	1.089	110.8	0.72977 ± 2	1.179 ± 11	n.d	0.648 ± 6	1413 ± 21	n.d
	Buds	HP-B	05/05/2005	5057	21872	533	11.7	7.28	1.104	3.495	80.19	0.72726 ± 8	1.192 ± 5	n.d	0.95 ± 1	217 ± 3	n.d
	Leaves (180 cm high)	HP-L2	13/09/2005	6698	9520	743	17.1	9.86	3.365	9.036	170.2	0.72744 ± 3	1.095 ± 4	1.03 ± 1	1.12 ± 1	151 ± 2	164 ± 2
	Top leaves	HP-SL	21/09/2005	5460	11253	738	7.63	5.82	2.449	7.380	71.97 (72.47)	0.72577 ± 1	1.074 ± 4	1.04 ± 1	1.00 ± 1	88 ± 1	84 ± 1
	Tree roots (Ø = 2-5 mm)	HP-MR	13/09/2005	2965	2324	108	27.7	10.6	7.307	16.82	262.2	0.72433 ± 3	1.133 ± 4	n.d	1.31 ± 1	107 ± 2	n.d
	Tree roots (Ø = 1-1.5 cm)	HP-SR	13/09/2005	1229	2114	67.1	13.0	5.38	16.75	47.09	120.8	0.72550 ± 2	1.149 ± 3	1.17 ± 1	1.08 ± 1	21.5 ± 3	19.8 ± 3
	Fine rootlets	HP-FR	13/09/2005	1419	2651	107	24.7	7.96	68.28	148.9	687.7	0.72518 ± 1	1.113 ± 3	1.34 ± 1	1.38 ± 1	30.1 ± 5	31.1 ± 5
	Top tree branches (Ø = 2-5 mm)	HP-TB	21/09/2005	2954	2311	290	22.8	8.92	0.879 (0.892)	2.070	70.46	0.72664 ± 1 (0.72672±8)	1.109 ± 4 (1.118±6)	n.d	1.28 ± 1	239 ± 4	n.d

U-Th-Ra italic data were determined by ICP-MS and the others by isotope dilution (n.d. : no defined). Replicates in brackets

Table 2a

	Ca Flux	(Ba/Ca)	(U/Ca)	(Th/Ca)	(Ra/Ca)	Ba flux	U flux	Th flux	Ra flux
	kg/m^2/a	□□/g	µg/g	µg/g	pg/g	µg/m^2/a	µg/m^2/a	µg/m^2/a	µg/m^2/a
Spruce Plot	12	0.8 - 4	1 - 5.3	3 - 15	4 - 16	900 - 1500	0.7 - 6	2 - 17	4.10^{-6} - $2. 10^{-5}$
Beech Plot	17.6	1.4 - 7.7	0.3 - 0.5	0.7 - 1.3	13 -25	2000 - 13000	0.5 - 1	1 - 2.3	2.10^{-5} - $4.5\ 10^{-5}$

Ba, U, Th and Ra fluxes are calculated by using the Ca flux given in Poszwa et al. (2000) and the range of Ba/Ca, U/Ca, Th/Ca and Ra/Ca concentrations ratios estimated for aerial parts (needles, leaves and branches) of trees analysed in each plot.

Table 2b

	Flux kg/m²/a	(U) µg/kg	(Th) µg/kg	(Ba) µg/kg	(Ra) g/kg	U flux µg/m²/a	Th flux µg/m²/a	Ba flux µg/m²/a	Ra flux µg/m²/a
Spruce (VP) plot : **Litter**[a]	0.3	*2.2*/19	*5.9*/59	*10.1*/13.8 *10³*	*4*	*0.7*/5.7	*1.8*/17.7	*3*/4.1 10^3	*0.62 10^{-5}*
Throughfall	1322	0.015±0.01	0.009±0.006	6±5	16	5.5±4	12±8	10±8 10^3	2.1 10^{-5}
soil solution (-5cm)	1246	0.03±0.01	0.11±0.05	13±6	59	37±17	137±65	16.6±8 10^3	7.3 10^{-5}
soil solution (-10cm)	1185	0.03±0.01	0.11±0.04	14±8	50	41±15	136±45	17.5±9.5 10^3	5.6 10^{-5}
soil solution (-30cm)	1119	0.03±0.01	0.04±0.01	30±9	7.5	32±7	48±11	35.±10.5 10^3	0.8 10^{-5}
soil solution (-60cm)	1107	0.012±0.01	0.005±0.004	10±4	22.6	13±10	6±4	11.3±4.2 10^3	2.5 10^{-5}
Beech (HP) Plot : **Litter**[b]	0.4	*3*/15	*8.2*/35	*12.3*/16 10^3	*140*	*1.2*/3	*3.3*/14	*4.9*/6.5 10^3	*17 10^{-5}*
Throughfall	1376	0.01±0.005	0.01±0.005	1.24±1	7.55	7±6	9±7	2±1.5 10^3	1.03 10^{-5}
soil solution (- 10cm)	1295	0.065±0.02	0.1±0.03	4.3±1.5	132	84±30	118±40	5.5±2 10^3	17 10^{-5}
soil solution (- 70cm)	1160	0.024±0.01	0.021±0.01	4.8±1.2	24	28±9	24±9	5.6±1.4 10^3	2.7 10^{-5}

A daily water balance model developed by Granier et al. (1999) has been used to estimate the soil drainage at different depths. This model simulates the dynamics of soil water depletion and recharge, and predicts the main components of forest water balance (at≈±10%). [a] Litter Flux in Ignatova and Dambrine, 2010 ; [b] Litter flux in Rihs et al., 2011. The U, Th, and Ba concentrations are the 2004-2006 mean annual concentrations and the standard deviation from data given in Table EA 1. The Ra concentration data are the average of the few analyses obtained in the present study. For the litters, the fluxes are calculated with the concentrations analyzed in the litter samples, which can contain some soil materials. If using leaf or needle data (in italic in table), the calculated U and Th fluxes would be ≈ one order of magnitude lower for U and Th.